Article

Neuron

A Missense Variant at the *Nrxn3* Locus Enhances Empathy Fear in the Mouse

Graphical Abstract

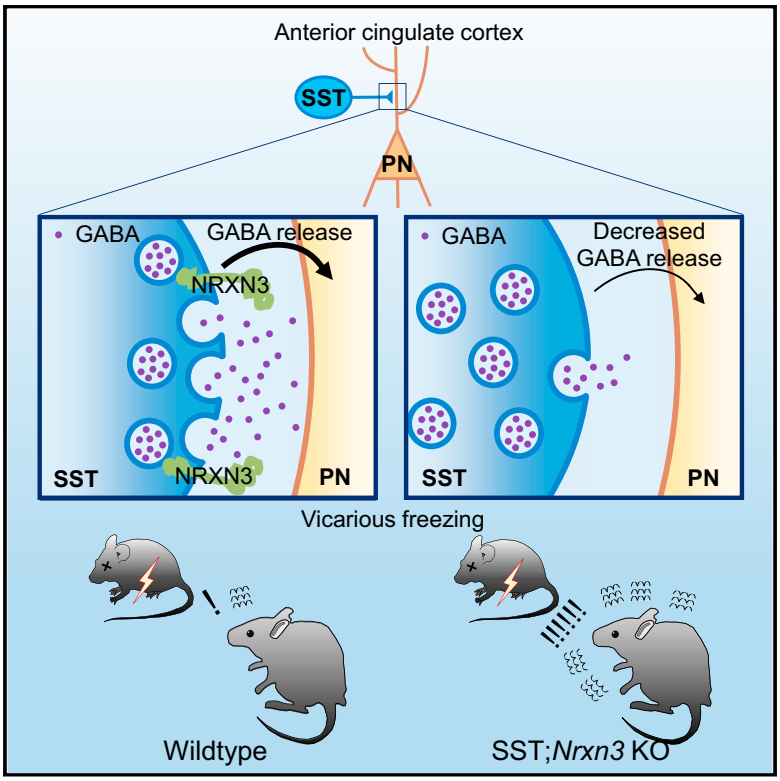

Authors

Sehoon Keum, Arie Kim, Jae Jin Shin, Jong-Hyun Kim, Joomin Park, Hee-Sup Shin

Correspondence

shin@ibs.re.kr

In Brief

Keum et al. demonstrate that a protein variant in the *Nrxn3* gene causes an enhancement in observational fear and that *Nrxn3*-dependent inhibitory synaptic functions in somatostatin-positive interneurons in the anterior cingulate cortex control the degree of empathy fear.

Highlights

- The 129S1 mouse strain exhibits a selective enhancement in observational fear
- A missense variant (R498W) in *Nrxn3* causes elevation of observational fear
- Selective deletion of *Nrxn3* in SST+ neurons reduces GABA release in the ACC
- SST+ inhibitory neurons in the ACC control the degree of socially transmitted fear

Keum et al., 2018, Neuron *98*, 588–601
May 2, 2018
https://doi.org/10.1016/j.neuron.2018.03.041

CellPress

CellPress

Neuron
Article

A Missense Variant at the *Nrxn3* Locus Enhances Empathy Fear in the Mouse

Sehoon Keum,[1,5] Arie Kim,[1,2,5] Jae Jin Shin,[1,3] Jong-Hyun Kim,[1,4] Joomin Park,[1,2] and Hee-Sup Shin[1,2,6,*]
[1]Center for Cognition and Sociality, Institute for Basic Science, Daejeon 34047, Republic of Korea
[2]School of Basic Science, University of Science and Technology, Daejeon 34113, Republic of Korea
[3]Department of Brain and Cognitive Science, Seoul National University, Seoul 08826, Republic of Korea
[4]Center for Glia-Neuron Interaction, Brain Science Institute, Korea Institute of Science and Technology, Seoul 02792, Republic of Korea
[5]These authors contributed equally
[6]Lead Contact
*Correspondence: shin@ibs.re.kr
https://doi.org/10.1016/j.neuron.2018.03.041

SUMMARY

Empathy is crucial for our emotional experience and social interactions, and its abnormalities manifest in various psychiatric disorders. Observational fear is a useful behavioral paradigm for assessing affective empathy in rodents. However, specific genes that regulate observational fear remain unknown. Here we showed that 129S1/SvImJ mice carrying a unique missense variant in neurexin 3 (*Nrxn3*) exhibited a profound and selective enhancement in observational fear. Using the CRISPR/Cas9 system, the arginine-to-tryptophan (R498W) change in *Nrxn3* was confirmed to be the causative variant. Selective deletion of *Nrxn3* in somatostatin-expressing (SST+) interneurons in the anterior cingulate cortex (ACC) markedly increased observational fear and impaired inhibitory synaptic transmission from SST+ neurons. Concordantly, optogenetic manipulation revealed that SST+ neurons in the ACC bidirectionally controlled the degree of socially transmitted fear. Together, these results provide insights into the genetic basis of behavioral variability and the neurophysiological mechanism controlling empathy in mammalian brains.

INTRODUCTION

Empathy is the ability to recognize and share the feelings of others. The neurocognitive processing of this affective and cognitive information is fundamental for our emotional and social lives (Bernhardt and Singer, 2012; de Waal, 2008). Either elevated or reduced empathy can contribute to difficulties in social interactions and mental well-being. Disturbance of empathy is a salient feature of many neuropsychiatric conditions, particularly autism spectrum disorders (ASDs) and psychopathy (Baron-Cohen and Wheelwright, 2004; Bora et al., 2008). Although there is a considerable genetic contribution to individual variability in empathy (Ebstein et al., 2010; Knafo et al., 2009; Rodrigues et al., 2009; Warrier et al., 2017), identification of specific genes that determine individual variability in empathy has been largely limited, primarily because it is difficult to control the social context in humans.

Recent evidence shows that empathy is evolutionarily conserved from rodents to humans (de Waal and Preston, 2017; Decety, 2011). Rodents possess a remarkable affective sensitivity to the emotional state of others and show empathy-related behaviors such as observational fear, emotional contagion of pain, social buffering, and prosocial helping behaviors (Ben-Ami Bartal et al., 2011; Burkett et al., 2016; Church, 1959; Jeon et al., 2010; Langford et al., 2006). In particular, observational fear has been recognized as a useful behavioral model for assessing empathic fear capacity (Debiec and Olsson, 2017; Keum and Shin, 2016; Meyza et al., 2017; Panksepp and Lahvis, 2011; Sivaselvachandran et al., 2016). In observational fear, a mouse is vicariously conditioned for fear by observing a conspecific receiving aversive foot shocks. This phenomenon, referred to as emotional state-matching or affect sharing, was measured as socially transmitted fear (Chen et al., 2009; Jeon et al., 2010). Human performance in a similar observational fear learning process was correlated with trait measures of empathy (Haaker et al., 2017; Kleberg et al., 2015; Olsson et al., 2007), suggesting that social transfer of fear is a fundamental feature of empathy that is conserved across species (Olsson and Phelps, 2007; Panksepp and Panksepp, 2013). Brain imaging studies have contributed to the understanding of the neural circuitries involved in empathy. Specifically, the anterior cingulate cortex (ACC) is involved in empathic responses of pain or fear (Olsson et al., 2007; Singer et al., 2004). Likewise, the activity of the ACC is augmented in mice engaged in observational fear, and its role in the acquisition of vicarious freezing has been demonstrated using neuroanatomical lesions (Jeon et al., 2010; Kim et al., 2012). However, despite the accumulating information about executive neural circuitry controlling observational fear, specific genes that determine different presentations of empathy-related behaviors are poorly understood.

To address these issues, we recently surveyed multiple inbred mouse strains and found that the vicarious freezing response was highly variable among different strains,

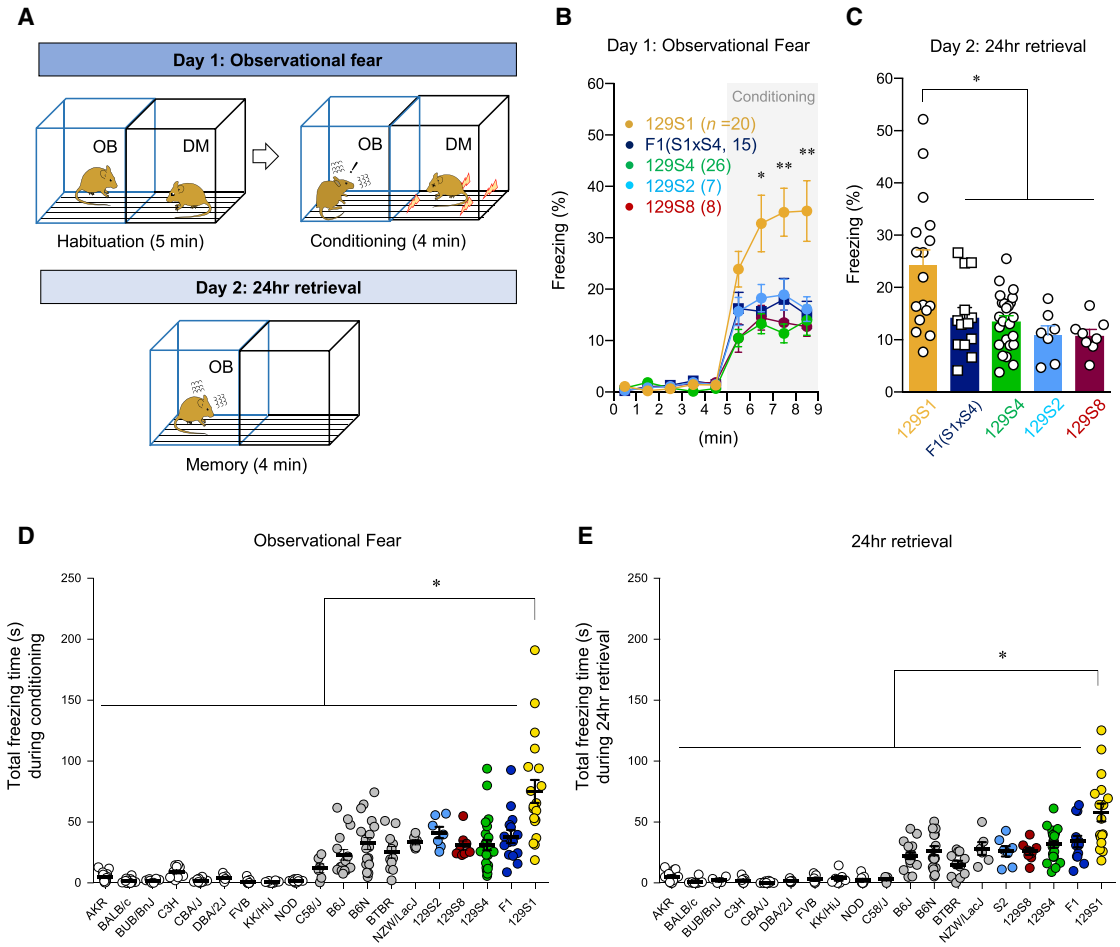

Figure 1. A Selective Enhancement in Observational Fear in 129S1 Mice

(A) Diagram of the observational fear chamber and outline of the behavioral paradigm. Day 1: conditioning. Observer (OB) and demonstrator (DM) mice are individually placed in the chamber and allowed to explore for 5 min (habituation). The observer mouse then witnesses a DM mouse receiving foot shocks through a transparent partition for 4 min (conditioning). Day 2: 24-hr retrieval. The observer mouse is returned alone to the same chamber in the absence of a DM mouse and shocks.

(B and C) Vicarious freezing of 129S1 (yellow), F1 (129S1xS4, navy), 129S2 (light blue), 129S4 (green), and 129S8 (magenta) observer mice was measured on day 1 (B), followed by measurement of 24-hr contextual memory (C). Strain 129S1 mice showed a marked increase in observational fear (S1, n = 18; S4, n = 26; two-way repeated measure [RM] ANOVA followed by Tukey's *post hoc* test, $F_{(1, 43)} = 14.06$, $p < 0.001$) and 24-hr memory compared with F1 mice and four other 129S substrains (Kruskal-Wallis one-way ANOVA on ranks followed by Dunn's test, $p < 0.05$).

(D and E) Distribution of total freezing time(s) during day 1 conditioning (D) and 24-hr memory (E) across 19 inbred strains of mice (AKR, n = 15; BALB/c, 14; BUB/BnJ, 8; C3H, 9; CBA/J, 10; DBA/2J, 9; FVB, 9; KK/HiJ, 8; non-obese diabetic [NOD], 10; C58/J, 6; B6J, 16; B6N, 23; BTBR, 14; NZW/LacJ, 6; 129S2, 7; 129S8, 8; 129S4, 26; F1, 14; 129S1, 18). The level of vicarious freezing in 129S1 mice was significantly higher than in any of the 18 other inbred mouse strains (Kruskal-Wallis one-way ANOVA on ranks by Dunn's test, $p < 0.05$).

All data are presented as means ± SEM. *$p < 0.05$, **$p < 0.01$, ***$p < 0.001$.

suggesting that the innate observational fear response is under genetic control (Keum et al., 2016). By comparing a panel of genetically nearly identical 129 Steel-lineage (129S) substrains, we identified that a missense variant in the *Nrxn3* gene present only in the 129S1/SvImJ (129S1) strain enhanced empathy fear. Using a combination of approaches, including cell type-specific ablation, *ex vivo* slice electrophysiology, and optogenetic manipulation, we demonstrate that *Nrxn3*-dependent somatostatin-expressing (SST+) interneurons in the ACC control the degree of social transfer of fear in mice.

RESULTS

The R498W Variant in *Nrxn3* Causes Elevation of Observation Fear

In the observational fear task, without receiving direct aversive stimuli, a mouse (observer) is vicariously conditioned for context-dependent fear by observing another mouse (demonstrator) receiving repetitive foot shocks (Figure 1A). Mice of the 129S1 inbred strain exhibited a marked increase in observational fear (Video S1) compared with other closely related 129S substrains, including 129S2/SvPas

(129S2), 129S4/SvJaeJ (129S4), and 129S8/SvEvNimrJ (129S8) (Figures 1B and 1C; Video S2). Surprisingly, we found that the level of observational fear response in 129S1 mice was significantly higher than that in any of the 17 other common inbred strains examined (Figures 1D and 1E). This elevated vicarious fear response in 129S1 mice did not significantly correlate with variation in locomotion, anxiety, or Pavlovian fear conditioning (Keum et al., 2016), leading us to hypothesize that this extreme phenotype in 129S1 mice was caused by observational fear-specific genetic variations unique to this strain.

To identify a causative variant, we performed whole-genome sequencing (WGS) of 129S1 and 129S4 strains (Table S1) and identified 32 non-synonymous coding SNPs in 23 genes that differed between 129S1 and 129S4 mice (Tables S2A and S2B). To further validate and identify 129S1-unique SNPs, we compared those 32 coding variants with published genome sequences of 17 inbred mouse strains (Keane et al., 2011). Only eight were 129S1-unique SNPs that distinguished the 129S1 strain from the other 17 strains (Table S3). We prioritized them based on the predicted consequences of the coding changes on the protein function and the mRNA abundance of the genes in the brain (STAR Methods). This analysis identified a homozygous non-synonymous SNP (rs241832271) that changes C to T at the 89,254,694 base pair (bp) on chromosome 12 as a top candidate to account for the altered behavioral phenotype of the 129S1 mice (Figure 2A). This SNP occurs in exon 6 of the neurexin 3 (*Nrxn3*) gene, encoding an evolutionarily conserved synaptic cell adhesion molecule that is essential for normal synapse assembly and synaptic transmission (Reissner et al., 2013; Südhof, 2008). The C-to-T change produces an arginine-to-tryptophan protein change at position 498 (R498W) in the third extracellular LNS (laminin-neurexin-sex hormone binding globulin) domain of NRXN3, which is highly conserved among vertebrates (Figures 2B and 2C). Notably, this change is predicted to be deleterious (Figure S1). The R498W variant was present only in 129S1 mice; none of the other inbred strains, including wild-derived mice, shared the T allele (Figure 2D; Table S2B), suggesting that this variant is not ancestrally inherited (Yang et al., 2011). To further pursue the historical origin of this variation, we performed DNA sequencing for the variant in an additional 129 substrains—129S2, 129S8, and 129T2—representing different genetic lineages (Figure 2E). The times of separation from the founder colony of these strains have been well documented (Festing et al., 1999; Simpson et al., 1997), allowing construction of a phylogenetic timeline of this *Nrxn3* variant (Figure 2F). Intriguingly, the R498W variant at the *Nrxn3* locus was fixed only in the 129S1 colony during selective breeding (Simpson et al., 1997) and was not present in most commercially available 129 strains. No 129S1-unique insertions or deletions (indels) or structural variants that caused protein coding changes were found.

To confirm that the R498W variant in *Nrxn3* caused elevated observational fear, we introduced the C > T non-synonymous change into B6J mice using CRISPR/Cas9 genome editing (Figure 3A). As expected, knockin (KI) mice harboring a homozygous Trp^{498} allele (KI-$Nrxn3^{WW}$) exhibited a significantly higher level of vicarious fear response than littermate wild-type (WT) mice (KI-$Nrxn3^{RR}$; Figure 3B). No difference was found in 24-hr memory between the two groups (Figure 3C). To further explore the effect of this coding variant on conditioned fear, we examined the KI-$Nrxn3^{WW}$ mice on a classical fear conditioning task but found no significant change in fear conditioning or 24-hr contextual fear memory (Figures 3D and 3E). Thus, the R498W variant in the *Nrxn3* gene specifically increased the degree of behavioral response of observer mice to the distress of demonstrator mice, indicating that KI-$Nrxn3^{WW}$ mice phenocopied the behavior of 129S1 mice.

SST+ Neuron-Specific Deletion of *Nrxn3* in the ACC Increases Observational Fear

The ACC was shown to be crucial for the acquisition of observational fear (Jeon et al., 2010; Kim et al., 2012). In the cortex, information processing depends on highly interconnected microcircuits composed of excitatory glutamatergic pyramidal and γ-aminobutyric acid-releasing (GABAergic) inhibitory neurons (Figure 4A) (Tremblay et al., 2016). Although the lack of high-affinity antibodies has hindered the assessment of *Nrxn3* protein expression (Reissner et al., 2013; Südhof, 2008), *in situ* hybridization and mRNA transcriptome studies have demonstrated that *Nrxn3* is highly expressed in the cortex (Aoto et al., 2013; Chen et al., 2017; Schreiner et al., 2014; Treutlein et al., 2014). In addition, *Nrxn3* shows distinct synaptic functions in different brain regions (Aoto et al., 2015). Thus, to elucidate the role of *Nrxn3* in observational fear, we used a cell type-specific targeting approach to dissect its specific involvement in distinct neuronal populations. First, to selectively delete *Nrxn3* in excitatory glutamatergic neurons of the forebrain, we generated conditional knockout (KO) mice by breeding mice that harbored a *Nrxn3* conditional allele ($Nrxn3^{f/f}$) with Emx1-Cre mice (Gorski et al., 2002) ($Emx1^{cre/+}$; $Nrxn3^{f/f}$, designated Emx1-*Nrxn3* KO). The Emx1-*Nrxn3* KO mice showed levels of observational fear similar to those of their WT littermates (Figure 4B). There was also no difference in 24-hr memory between the genotypes (Figure 4C). To confirm this, we deleted *Nrxn3* in putative excitatory cortical neurons by focally injecting an adeno-associated virus (AAV) expressing Cre recombinase under the control of the calcium/calmodulin-dependent protein kinase IIα promotor (AAV-*Camk2*α-Cre) into the ACC of $Nrxn3^{f/f}$ mice (Figure S2A). Similar to Emx1-*Nrxn3* KO mice, observer mice with a localized *Nrxn3* deletion in excitatory neurons in the ACC exhibited no difference in either acquisition or 24-hr memory of observational fear compared with control mice (Figures S2B and S3C), indicating that *Nrxn3* in cortical pyramidal neurons is not critically involved in the regulation of observational fear.

Next, to examine the role of *Nrxn3* in GABAergic inhibitory neuron populations, we first crossed conditional $Nrxn3^{f/f}$ mice with pan-GABAergic Vgat-Cre mice in which Cre recombinase is expressed under the control of the GABA vesicular transporter (*Slc32a1*) (Vong et al., 2011). However, we found that, when crossed to homozygosity, Vgat-*Nrxn3* KO mice were not viable (live births: 20 WT, 47 heterozygous, and 0 homozygous KO), consistent with a previous report that germline *Nrxn3*-KO mice die at birth (Aoto et al., 2015). These results underscored the possibility that *Nrxn3* plays a critical role in GABAergic synapse development. This finding prompted us to further explore the consequence of *Nrxn3* ablation on the synaptic function of

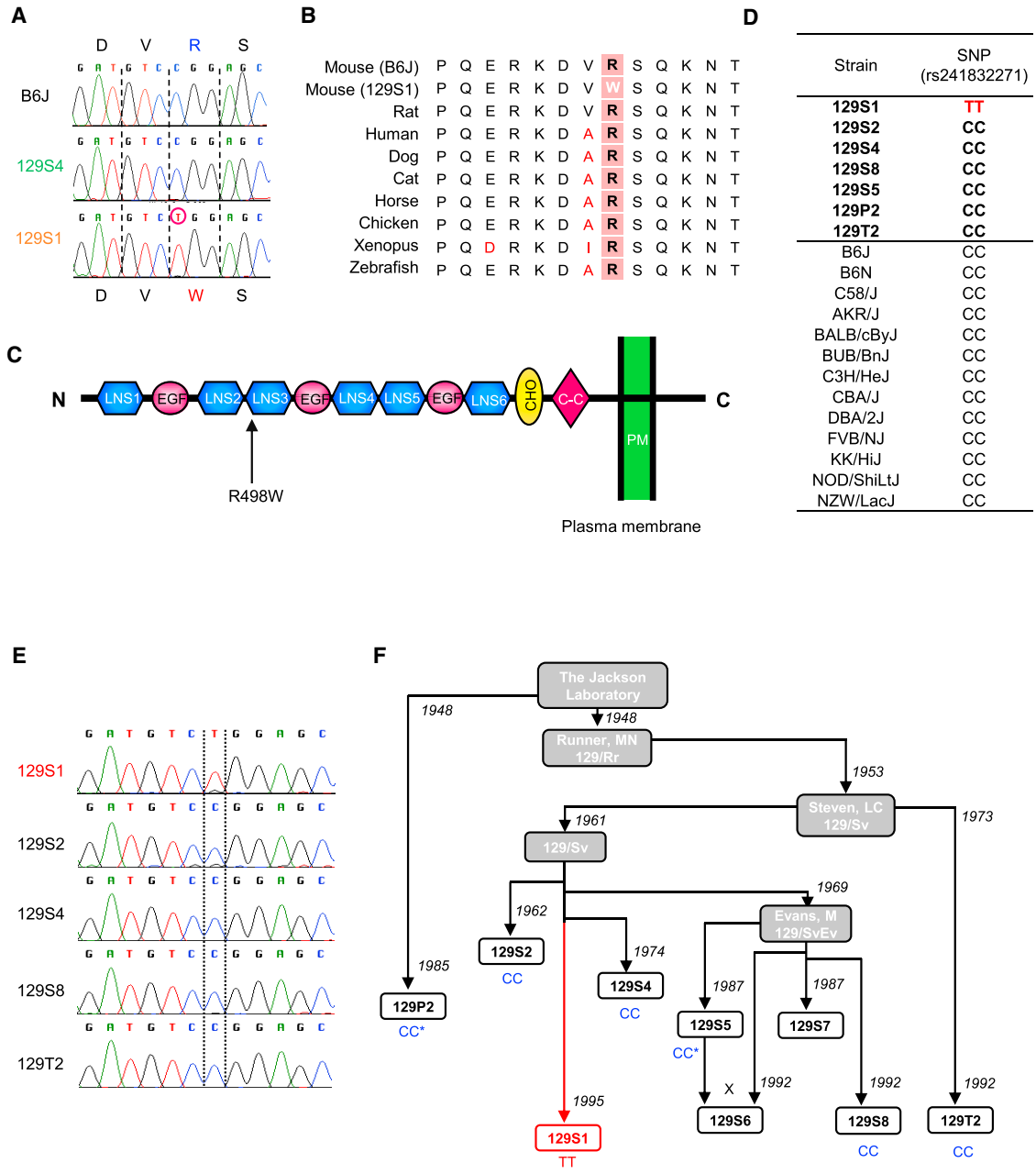

Figure 2. The 129S1-Unique R498W Variant in the *Nrxn3* Gene

(A) Direct DNA sequencing of exon 6 of the *Nrxn3* gene in the B6J, 129S4, and 129S1 strains.

(B) Phylogenetic conservation of the exon 6-encoded LNS3 domain of NRXN3. The R498W variant occurs at a residue that is conserved among vertebrates.

(C) Structure of NRXN3 and location of the R498W variant. LNS, laminin G-neurexin-sex hormone-binding globulin domain; EGF, epidermal growth factor-like repeat; CHO, carbohydrate-attachment sequence; C-C, cysteine loop.

(D) Comparison of SNP rs241832271 in 20 inbred mouse strains.

(E) Direct DNA sequencing of exon 6 of the *Nrxn3* gene in five 129 substrains.

(F) A phylogenetic timeline of the R498W *Nrxn3* variant; 129P2 (129P2/OlaHsd), 129S2 (129S2/SvPas), 129S4 (129S4/SvJae), 129S5 (129S5/SvEvBrd), 129S7 (129S7/SvEvBrd-Hprt1b-m2), 129S8 (129S8/SvEv-Gpi1c Hprt1b-m2/J), 129T2 (129T2/SvEms), and 129S1 (129Sv/SvImJ). *Sequence data obtained from the Sanger genome database (http://www.sanger.ac.uk/sanger/Mouse_SnpViewer/rel-1410).

specific GABAergic inhibitory neuronal populations. To this end, we generated three lines of conditional KO mice lacking *Nrxn3* in parvalbumin-expressing (PV+) neurons (PV-*Nrxn3* KO), SST+ neurons (SST-*Nrxn3* KO), or vasoactive intestinal peptide-expressing (VIP+) neurons (VIP-*Nrxn3* KO) by crossing *Nrxn3*$^{f/f}$ mice with PV-Cre, SST-Cre, or VIP-Cre mice, respectively,

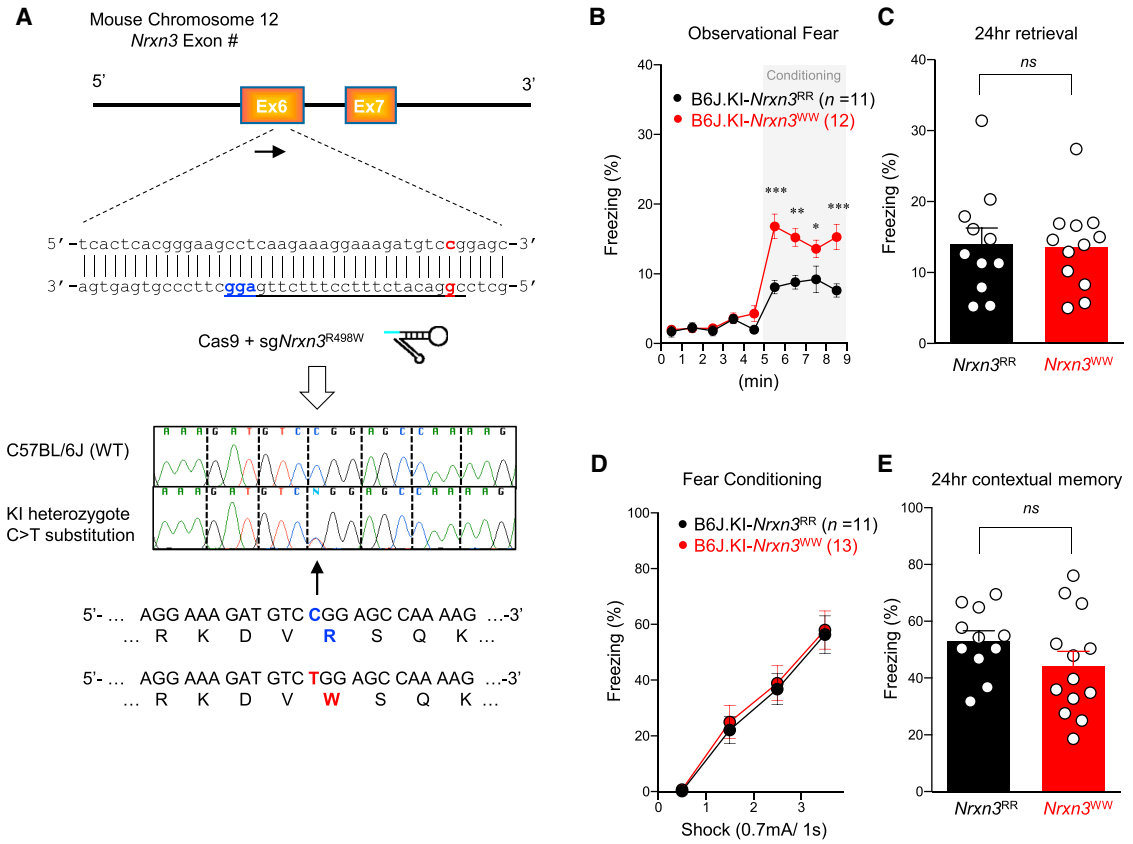

Figure 3. *Nrxn3* KI Observer Mice Show Increased Vicarious Fear

(A) Schematic illustration of the target site at exon 6 of the mouse *Nrxn3* locus. In the double-stranded DNA, the protospacer adjacent motif (PAM) sequence (blue) and the single-guide RNA (sgRNA) target are underlined. Sequence chromatograms for the target site of WT (top) and heterozygote KI (bottom) founder mice show a mono-allelic C-to-T substitution (the overlapping peak). The deduced amino acid sequences from WT and substituted sequences are shown at the bottom, with red letters indicating the result of the R498W substitution.

(B) KI-*Nrxn3*^{WW} mice (n = 12) showed higher responses in observational fear than WT KI-*Nrxn3*^{RR} (n = 11) littermates (two-way RM ANOVA followed by Tukey's *post hoc* test, $F_{(1, 22)} = 20.67$, $p < 0.001$).

(C) No difference in 24-hr contextual memory between KI-*Nrxn3*^{WW} and WT mice.

(D) KI-*Nrxn3*^{WW} mice (n = 13) show no difference in conditioned fear over trials compared with WT littermate (n = 11) controls.

(E) The level of 24-hr contextual fear memory in KI-*Nrxn3*^{WW} mice (n = 13) is similar to that of WT mice (n = 11).

Data are presented as means ± SEM. *p < 0.05; **p < 0.01; ***p < 0.001; ns, not significant.

representing the majority (>80%) of the GABAergic neuronal population in the cortex (Hippenmeyer et al., 2005; Taniguchi et al., 2011; Tremblay et al., 2016). Strikingly, we found that SST-*Nrxn3* KO observer mice showed greatly increased vicarious freezing compared with their WT littermates (Figure 4D; Video S3). 24-hr memory was also significantly higher in SST-*Nrxn3* KO mice compared with WT mice (Figure 4E). By contrast, both PV-*Nrxn3* KO and VIP-*Nrxn3* KO mice exhibited no difference in observational fear compared with their WT controls (Figures 4F–4I). We tested SST-*Nrxn3* KO mice on a classical fear conditioning task but found no difference between the KO and WT mice (Figures S3A and S3B), highlighting the specific role of *Nrxn3* in SST+ neurons in the modulation of observational fear. Next, we examined whether the elevated observational fear in SST-*Nrxn3* KO mice was due to the loss of *Nrxn3* in SST+ neurons in the ACC, which is integral to the acquisition of vicarious fear (Jeon et al., 2010; Kim et al., 2012). To this end, we bred SST-Flp;*Nrxn3*$^{f/f}$ mice, in which flippase (Flp) recombinase was selectively expressed in SST+ neurons in a *Nrxn3*$^{f/f}$ genetic background, and injected the ACC of these mice with an AAV expressing Cre recombinase in a Flp-dependent manner with a double-floxed inverted open reading frame (AAV-fDIO-Cre). This approach allowed SST+ neuron-specific deletion of *Nrxn3* restricted to the ACC area (Figure 4J). Indeed, we found that this resulted in elevated vicarious fear responses (Figures 4K and 4L), a phenotype that resembled that of the SST-*Nrxn3* KO mice. Thus, the lack of *Nrxn3* in SST+ neurons in the ACC caused elevation of observational fear.

Reduced GABAergic Transmission from SST+ Neurons Lacking *Nrxn3*

SST+ interneurons primarily target distal dendrites of pyramidal cells and have a prominent role in regulating distal dendritic excitability (Chiu et al., 2013; Dumitriu et al., 2007; Gentet

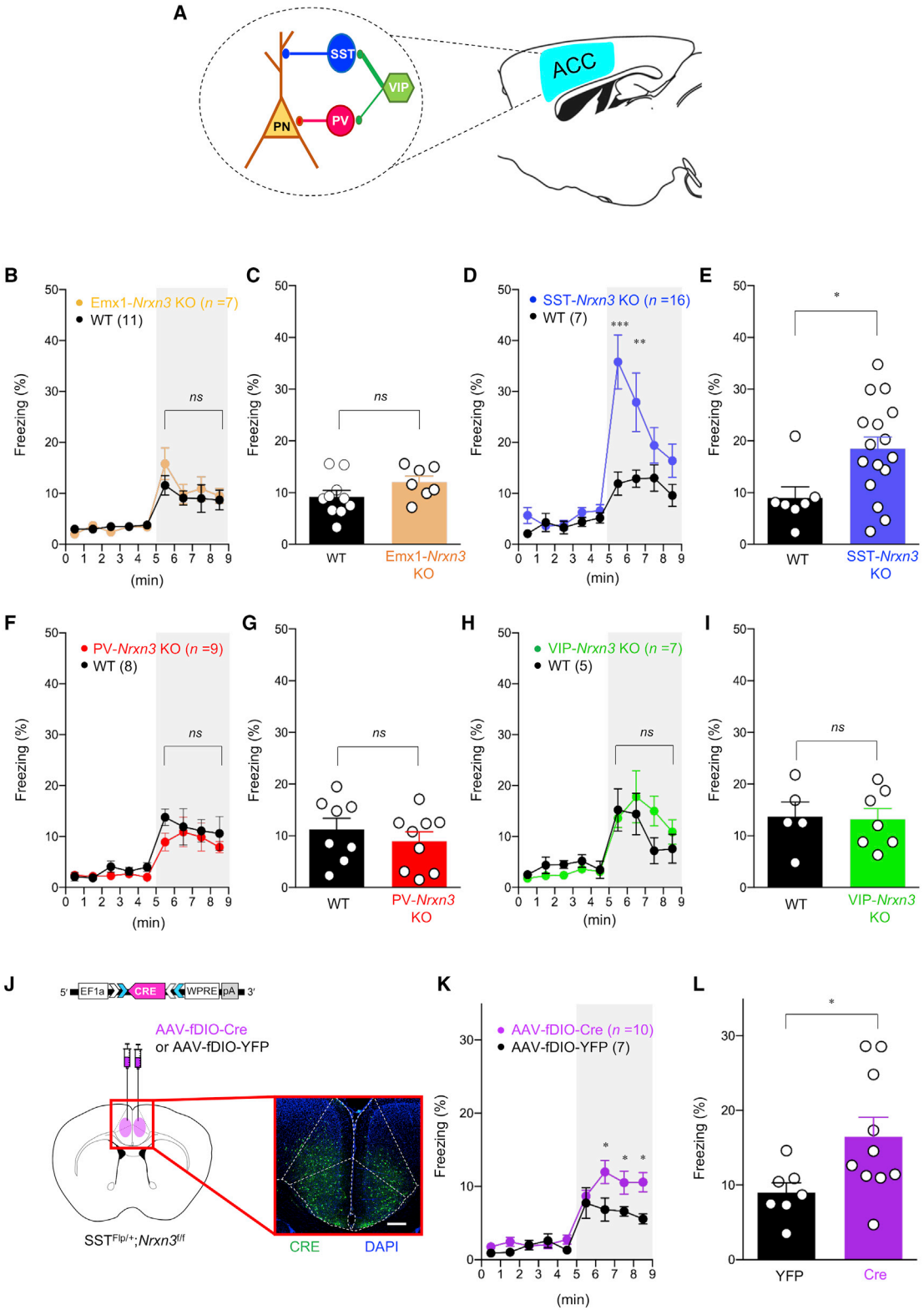

Figure 4. Loss of *Nrxn3* in SST+ Neurons in the ACC Increases Observational Fear

(A) Schematic overview of the major neuronal populations of the microcircuit in the ACC. Yellow triangle, pyramidal neurons (PNs); red circle, PV+ interneurons; blue ellipse, SST+ interneurons; green hexagon, VIP+ interneurons.

(legend continued on next page)

et al., 2012; Urban-Ciecko et al., 2015). Thus, we measured synaptic functions in SST-*Nrxn3* KO mice by performing whole-cell patch-clamp recordings in layer 2/3 (L2/3) of the right ACC in acute brain slices. Given that interneuron activity-dependent inhibition tightly modulates the output of excitatory neurons, we first measured the intrinsic excitability of putative pyramidal neurons and SST+ interneurons in SST-*Nrxn3* KO mice. To identify SST+ interneurons, we crossed SST-*Nrxn3* KO mice with a Cre-dependent Rosa26$^{LSL\text{-}tdTomato}$ (*Ai14*) reporter line (SST$^{cre/+}$;*Nrxn3*$^{f/f}$;*Ai14*$^{f/+}$) to label SST+ neurons with a red fluorescent protein (Madisen et al., 2010). All recorded putative pyramidal cells exhibited a regular adaptation firing discharge pattern, and their average frequency of action potential discharge at incremental step current injections was similar between WT and SST-*Nrxn3* KO mice (Figures S4A and S4B). SST+ interneurons lacking *Nrxn3* also showed no difference in intrinsic excitability (Figures S4C and S4D).

To examine inhibitory synaptic transmission, we measured miniature inhibitory postsynaptic currents (mIPSCs) from L2/3 pyramidal neurons of the ACC (Figure 5A). SST-*Nrxn3* KO mice showed a significant decrease in mIPSC frequency, but not amplitude, suggesting that presynaptic GABA release probability was reduced (Figures 5B and 5C). To determine whether loss of presynaptic *Nrxn3* in SST+ neurons affected GABAergic transmission onto pyramidal neurons, we performed dual whole-cell patch-clamp recordings on pairs of neighboring SST+ neurons and pyramidal cells (Figure 5D). Paired recordings demonstrated a substantial deficit in inhibitory synaptic transmission in the ACC of SST-*Nrxn3* KO mice (Figure 5E). We observed a marked reduction (~50%) in the amplitude of action potential (AP)-evoked IPSCs (eIPSCs) from SST+ neurons onto pyramidal neurons in the SST-*Nrxn3* KO mice (Figure 5F). We recorded paired-pulse depression (PPD) of inhibitory synaptic inputs on pyramidal neurons and calculated the paired-pulse ratio of eIPSCs. We found that the PPD between the two eIPSCs with 50-ms interval was significantly different between WT and SST-*Nrxn3* KO mice (76.94% ± 5.68 (WT) versus 99.05 ± 1.20 (KO), $p < 0.001$). Collectively, *Nrxn3* ablation in SST+ neurons decreased the efficacy with which an AP triggers GABA release onto L2/3 pyramidal neurons in the ACC. Examination of excitatory synaptic transmission by recording miniature excitatory postsynaptic currents (mEPSCs) in both L2/3 pyramidal cells and SST+ interneurons revealed no significant change in amplitude or frequency of excitatory events in SST-*Nrxn3* KO mice (Figures S5A–S5F).

SST+ Neurons, but Not PV+ Neurons, Control the Degree of Observational Fear Response in the ACC

Our electrophysiological data suggested that the reduced inhibitory synaptic transmission from SST+ neurons contributes substantially to the hyperactivity of excitatory pyramidal neurons and, thereby, drives enhanced vicarious fear to the distress of demonstrators. To determine the contribution of the activity of SST+ interneurons in observational fear, we asked whether acute inactivation of SST+ neurons in the ACC would alter vicarious freezing in observer mice. To this end, we injected an AAV expressing the Cre-dependent, engineered chloride (Cl^-) pump, halorhodopsin (AAV-DIO-eNpHR3.0-YFP [yellow fluorescent protein]) into the right ACC of SST-Cre and PV-Cre mice to selectively label SST+ or PV+ interneurons, respectively (Tremblay et al., 2016; Figures 6A, 6D, and S6A–S6F). Strikingly, optogenetic suppression of SST+ neurons in the right ACC during conditioning evoked an increase in freezing responses compared with control mice, mimicking SST-*Nrxn3* KO (Figures 6B and 6C; Video S4). Importantly, similar suppression of PV+ neurons had no effect (Figures 6E and 6F), revealing that SST+ neurons, but not PV+ neurons, were critically involved in this process. We then tested whether activation of SST+ neurons affects the level of observational fear using an AAV expressing Cre-dependent channelrhodopsin (AAV-DIO-ChR-YFP; Figure 6G). We found that the effect of activating SST+ neurons in the right ACC was robust and almost completely abolished the acquisition of vicarious freezing (Figure 6H; Video S5). There was also a significant reduction in 24-hr context memory in SST-Cre mice following optogenetic activation (Figure 6I). These results suggest that the activity level of SST+ neurons in the right ACC can bidirectionally modulate the level of vicarious freezing.

DISCUSSION

In this study, we have attempted to identify a specific genetic determinant critical to observational fear, an empathy-related behavior in mice, by exploiting naturally occurring phenotypic differences between genetically closely related 129S substrains. We discovered that a protein-altering variant of the *Nrxn*3 gene specific to the 129S1 strain enhanced observational fear. Importantly, 129S1 mice exhibited vicarious fear significantly higher than that of other 129S substrains or any of 17 other common inbred strains, indicating that this phenotypic abnormality was very specific to the 129S1 strain. Both nearly identical genetic

(B and C) PN-specific deletion of *Nrxn3* in Emx1-*Nrxn3* KO mice (n = 7) had no effect on observational fear (B) and 24-hr retrieval (C) compared with that observed in WT littermates (n = 11).

(D) Deletion of *Nrxn3* in SST+ neurons increased vicarious freezing in observational fear conditioning (SST-*Nrxn3* KO, n = 16; WT littermates, n = 7; two-way RM ANOVA followed by Tukey's *post hoc* test, $F_{(1, 22)} = 7.34$, $p < 0.001$).

(E) SST-*Nrxn3* KO mice showed an increase in freezing in 24-hr retrieval (one-way ANOVA followed by Tukey's *post hoc* test, $F_{(1, 22)} = 7.68$, $p = 0.011$).

(F and G) PV-*Nrxn3* KO mice (n = 9) showed no difference in observational fear (F) and 24-hr memory (G) compared with WT littermates (n = 8).

(H and I) Mice with VIP interneuron-specific deletion of *Nrxn3* (n = 7) exhibited similar observational fear (H) and 24-hr retrieval (I) compared with WT littermates (n = 5).

(J) Bilateral injection of AAV-fDIO-Cre to selectively delete *Nrxn3* in SST+ neurons in the ACC and a representative confocal image of the ACC of an SST-flp;*Nrxn3*$^{f/f}$ mouse in which the virus was injected into the right ACC (blue, DAPI; green, CRE [Cre-recombinase]). Scale bar, 200 μm.

(K and L) Selective deletion of *Nrxn3* in SST+ neurons in the ACC increased both observational fear (K) (AAV-fDIO-Cre, n = 10; control AAV-fDIO-YFP, n = 7; two-way RM ANOVA followed by Tukey's *post hoc* test, $F_{(1, 16)} = 4.73$, $p = 0.043$) and 24-hr memory (L) (one-way ANOVA followed by Tukey's post hoc test, $F_{(1, 16)} = 5.14$, $p = 0.039$).

Data are presented as means ± SEM. *$p < 0.05$, **$p < 0.01$, ***$p < 0.001$.

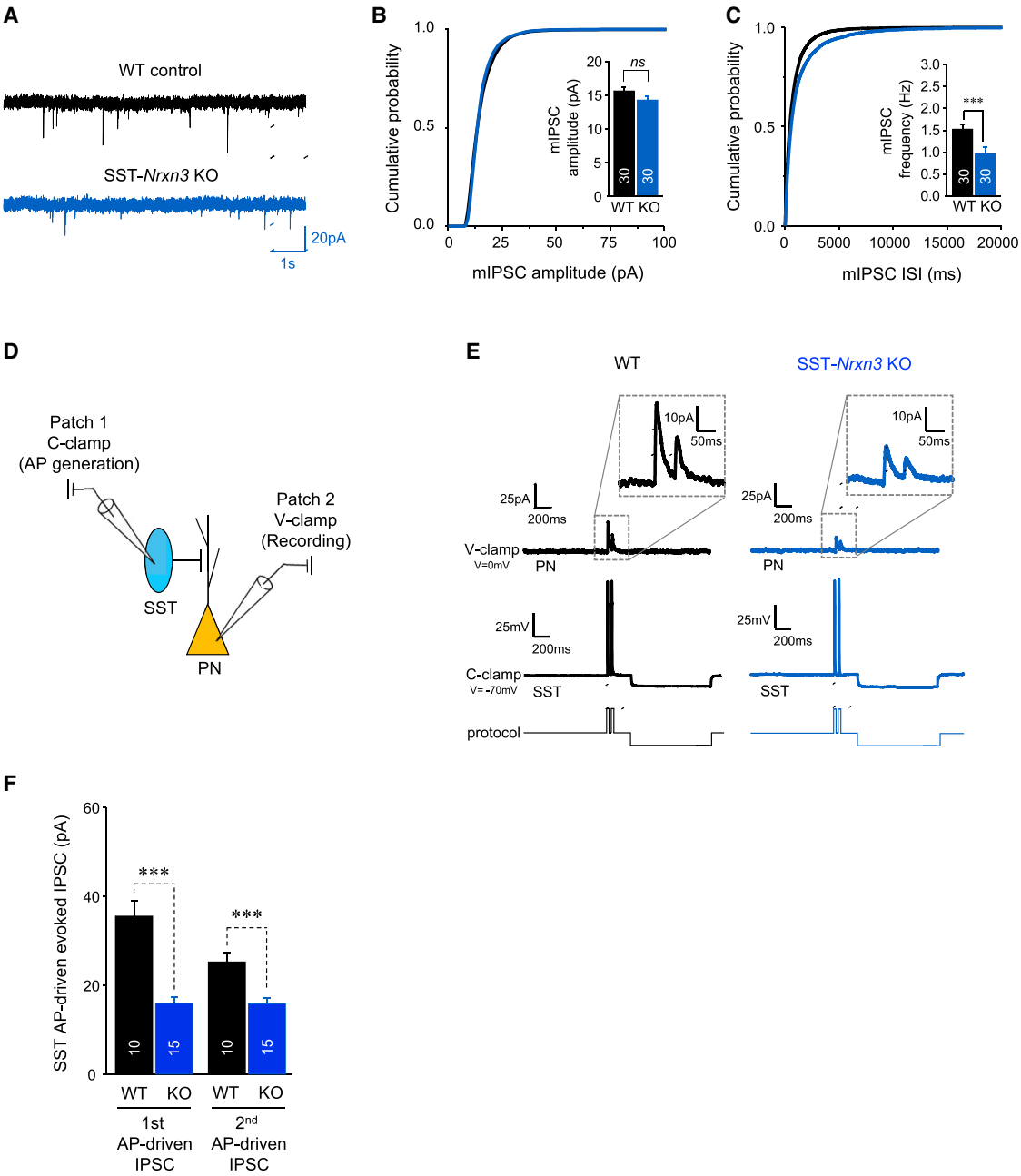

Figure 5. *Nrxn3* Is Essential for Inhibitory Synaptic Transmissions in SST+ Neurons

(A) Representative mIPSC traces from L2/3 PNs in the ACC of SST-*Nrxn3* KO and WT littermate mice.

(B) Cumulative probability plot of mIPSC amplitudes and a summary graph of the mean mIPSC amplitude (inset) recorded from WT (n = 30 cells) and SST-*Nrxn3* KO (n = 30 cells) mice.

(C) Cumulative probability plot of mIPSC inter-event intervals (ISIs) and a summary graph of the mean mIPSC frequency (inset) recorded from WT (n = 30 cells) and SST-*Nrxn3* KO (n = 30 cells) mice. SST-*Nrxn3* KO mice showed a significant reduction in mIPSC frequency (two-tailed t-test, $p < 0.001$).

(D) Schematic diagram of the paired recording configuration for measuring inhibitory synaptic transmission from SST+ interneurons onto the distal dendrites of L2/3 PNs. SST+ neurons in the ACC were identified in slices based on Cre-dependent tdTomato red fluorescence (*Ai14*).

(E) Representative paired whole-cell recording traces showing a monosynaptic connection between an SST+ cell and a PN from a WT (left, black) and an SST-*Nrxn3* KO (right, blue) mouse. IPSCs were evoked by generating two individual APs with a 50-ms interval through current injection into patched presynaptic SST+ neurons (bottom, SST) and were recorded from patched postsynaptic PN (top) traces.

(F) A summary plot of evoked IPSC amplitudes recorded from WT (n = 10 cells) and SST-*Nrxn3* KO (n = 15 cells) mice. GABAergic synaptic strength was significantly reduced in SST+ neurons lacking *Nrxn3* (two-way ANOVA followed by Bonferroni *post hoc* test, $F_{(1,24)} = 21.26$, $p < 0.001$).

Data are presented as means ± SEM. *$p < 0.05$, ***$p < 0.001$.

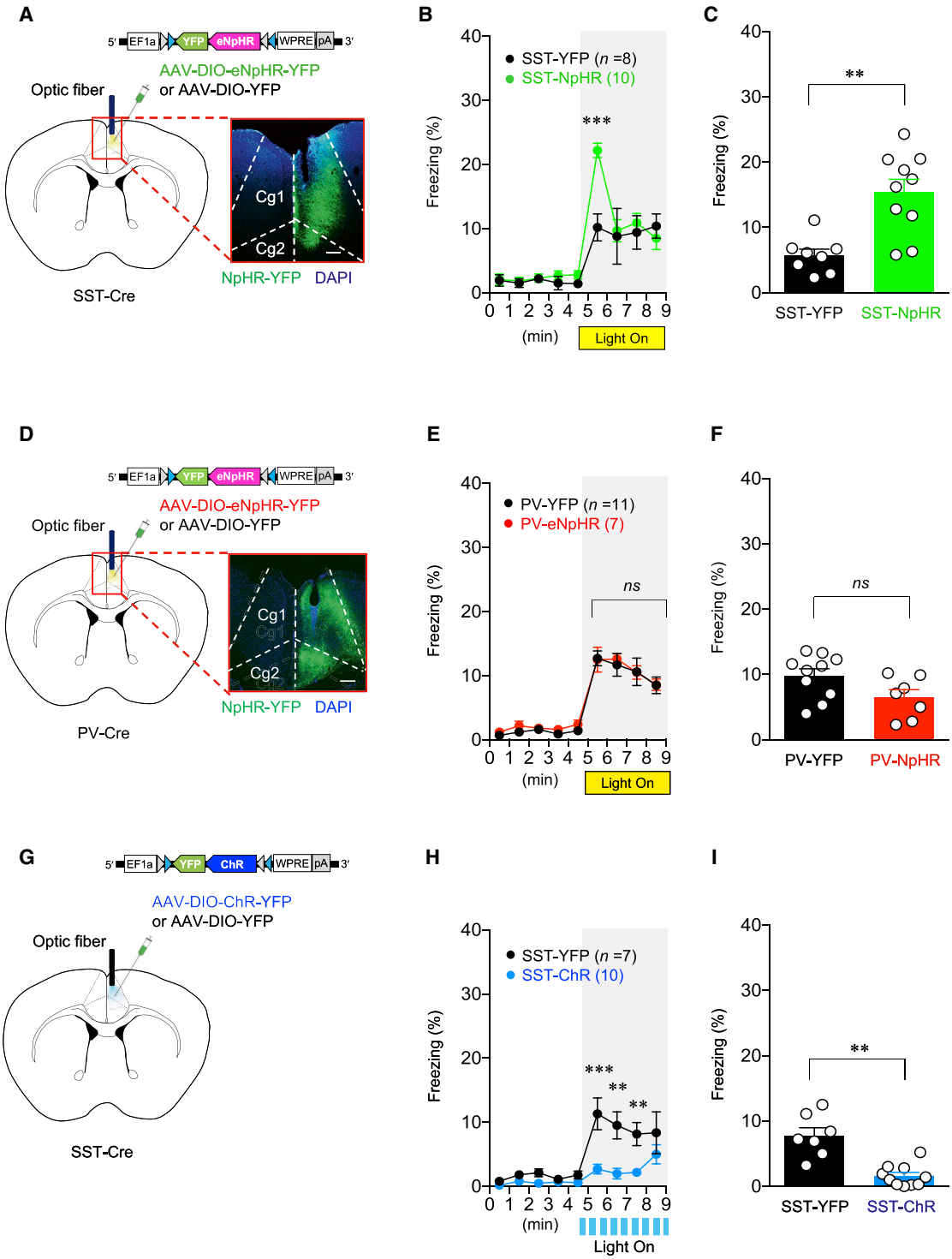

Figure 6. SST+ Neurons in the ACC Control the Degree of Observational Fear Response

(A) Injection and implantation strategy for optogenetic suppression of SST+ neurons in the ACC and a representative confocal image of optic fiber placement in the right ACC of an SST-Cre mouse injected with AAV-DIO-eNpHR-YFP (blue, DAPI; green, NpHR-YFP). Cg, cingulate cortex. Bregma, 1.0 mm. Scale bar, 200 μm.

(B) Vicarious freezing was elevated by optogenetic inhibition of SST+ interneurons (SST-YFP control, n = 8; SST-NpHR, n = 10; two-way RM ANOVA followed by Turkey's *post hoc* test, $F_{(1, 17)} = 16.96$, $p < 0.001$).

(legend continued on next page)

variations between the 129S substrains and the extreme phenotype of 129S1 mice significantly expedited the discovery of the underlying causative variant. Using CRISPR/Cas9 genome editing, we confirmed that the R498W variant of the *Nrxn3* gene increased observational fear in the B6J background. Thus, our study offers an important framework for utilizing mouse substrains to identify a novel function of a gene that regulates a complex behavioral trait. Previous studies demonstrated that 129S1 mice exhibited impaired fear extinction in association with functional abnormalities in a cortico-amygdala circuit (Camp et al., 2009, 2012; Hefner et al., 2008). The 129S1 mouse strain was developed to serve as a control strain for many of the steel lineage-derived embryonic stem cell (ESC) lines (Festing et al., 1999; Simpson et al., 1997). To avoid potential confounds caused by the R498W variant in the *Nrxn3* gene, care should be taken in future behavioral studies when examining the role of a targeted gene mutation produced in 129S1-derived ESC lines.

Historically, spontaneous mutations have revealed novel functions for known genes, often implicating biological processes previously unknown or only suspected to be involved in the trait. Although the R498W variant in *Nrxn3* was validated as a causative variant, at present we cannot explain exactly how this coding change contributes to the function of the protein in the synapse. We found no difference in the *Nrxn3* mRNA level in the cortex between KI-*Nrxn3*^{RR} (WT) and KI-*Nrxn3*^{WW} mice (Figure S7), suggesting that the R498W coding variant may disrupt protein stability or ligand binding, resulting in impaired synaptic functions. The R498W variant is located in the third extracellular LNS domain (αLNS3), a region of the protein thought to be involved in the Ca^{2+}-mediated conformational switch for ligand binding (Chen et al., 2011; Miller et al., 2011). Currently, only two extracellular ligands—neurexophilins and dystroglycan—were identified, both of which bind to the αLNS2 domain (Missler et al., 1998; Sugita et al., 2001). To date, no binding partners for the αLNS3 domains of neurexins have been identified (Südhof, 2017). Nonetheless, because SST-*Nrxn3* KO mice appeared similar to 129S1 and KI-*Nrxn3*^{WW} mice, and loss of function of SST+ neurons using optogenetic inactivation also increased vicarious freezing, we surmise that the net effect of the Trp^{498} allele is at least a partial loss of function. Recent mRNA transcriptome profiling studies revealed that enormously diverse variants of the *Nrxn3* transcript were expressed in distinct cell populations by highly differential, cell type-specific alternative splicing (Fuccillo et al., 2015; Schreiner et al., 2014; Treutlein et al., 2014). However, because exon 6, which harbors the R498W protein change, is not subject to canonical alternative splicing (Treutlein et al., 2014), the Trp^{498} allele in 129S1 mice may affect a majority of the NRXN3 proteins (~98%).

It should be noted that, despite its elevated vicarious freezing response, we observed that the KI-*Nrxn3*^{WW} mice showed no difference in 24-hr retrieval compared with the KI-*Nrxn3*^{RR} WT controls. Intriguingly, recent studies showed that neurexins are not simple building blocks of all synapses but, rather. play distinct roles in different brain regions (Chen et al., 2017; Südhof, 2017). Specifically, *Nrxn3* is necessary for GABA release in the olfactory bulbs and α-amino-3-hydroxy-5-methyl-4-isoxazole-propionic acid (AMPA) receptor stabilization in the hippocampus through its interactions with multiple synaptic adhesion molecules (Aoto et al., 2013, 2015). Because we had introduced the 129S1-specific Trp^{498} allele into the B6J genetic background, this phenotypic dissociation in the KI-*Nrxn3*^{WW} mice could have been caused by "modifier genes" involved in neural circuits underlying the formation or retrieval of social fear memory.

Nrxn3 is abundantly expressed in inhibitory neurons, including cortical SST+ and PV+ neurons (Chen et al., 2017; Paul et al., 2017; Ullrich et al., 1995), but its role has never been defined in different cell types or explored in social behaviors in mice. In this study, we found that *Nrxn3* was selectively required for inhibitory synaptic transmission in SST+ interneurons in the ACC. Thus, dysfunctional inhibitory circuits in the ACC of SST-*Nrxn3* KO mice caused hyperactivity of excitatory pyramidal neurons, resulting in elevated observational fear response to the distress of demonstrators. This was the first study to characterize the cell type-specific role of *Nrxn3* and identify a novel role of *Nrxn3*-dependent SST+ neurons in the ACC in controlling socially transmitted fear in rodents. In addition to the ACC, we have previously demonstrated that the mediodorsal and parafascicular thalamic nuclei, which are part of the affective pain system, are necessary for acquisition of observational fear (Jeon et al., 2010). Because *in situ* hybridization studies showed that *Nrxn3* is highly expressed in the cortex but undetected or expressed at a very low level in these thalamic nuclei (http://mouse.brain-map.org/experiment/show/75042240; Ullrich et al., 1995), we hypothesized that the enhanced vicarious freezing in SST-*Nrxn3* KO mice was due to defective *Nrxn3* signaling in SST+ neurons in the ACC. Indeed, using AAV-fDIO-Cre, we found that deletion of *Nrxn3* restricted to SST+ neurons in the ACC increased observational fear. These results suggest that the behavioral enhancement in mice with the *Nrxn3* R498W variant or SST-specific *Nrxn3* KO was largely due to its role in the ACC.

Deletion mutations in the *NRXN3* gene were directly implicated as a genetic risk factor for ASDs (Vaags et al., 2012). Although mice with *Nrxn3* mutations exhibited elevated empathy fear, human autism is commonly diagnosed with reduced affective empathic responses (Baron-Cohen and Wheelwright, 2004; Peterson, 2014). However, other studies show that emotional

(C) Optogenetic inactivation of SST+ neurons during day 1 conditioning resulted in increased freezing in 24-hr contextual memory (one-way ANOVA followed by Turkey's *post hoc* test, $F_{(1, 17)} = 17.04$, $p < 0.001$).

(D) Injection and implantation strategy for optogenetic inhibition of PV+ interneurons in the ACC and a representative confocal image of optic fiber placement in the right ACC of a PV-Cre mouse injected with AAV-DIO-eNpHR-YFP (blue, DAPI; green, NpHR-YFP). Bregma, 1.0 mm rostral. Scale bar, 200 μm.

(E and F) Mice with optogenetic suppression of PV+ neurons (PV-NpHR, n = 7) show no difference in observational fear (E) and 24-hr retrieval (F) compared with control mice (PV-YFP, n = 11).

(G) Injection and implantation strategy for optogenetic activation of SST+ neurons in the ACC.

(H and I) Optogenetic stimulation of SST+ neurons in the ACC decreased observational fear (H) (SST-YFP control, n = 7; SST-ChR, n = 10; two-way RM ANOVA followed by Turkey's *post hoc* test, $F_{(1, 16)} = 10.14$, $p = 0.006$) and 24-hr memory (I) (one-way ANOVA followed by Turkey's *post hoc* test, $F_{(1, 16)} = 26.66$, $p < 0.001$). All data are presented as means ± SEM. *$p < 0.05$, **$p < 0.01$, ***$p < 0.001$.

empathic response can be intact, or even heightened, in ASDs (Bernhardt et al., 2014; Bird et al., 2010). Intriguingly, a recently published work demonstrated that participants high in autistic traits showed an elevated observational fear response (Kleberg et al., 2015). This heterogeneity suggests a more general affective imbalance in neurocognitive capacity in patients with ASDs (Bird et al., 2010; Markram et al., 2007). Because neurexins mediate synaptic connectivity (Südhof, 2017), dysfunction of *Nrxn3* in SST+ or other types of neurons may perturb the neural circuitry underlying social interactions and repetitive behaviors at different nodes in ASD patients (Courchesne and Pierce, 2005; Hahamy et al., 2015; Sahin and Sur, 2015). Similarly, a locus in 3p26.1 was significantly associated with cognitive empathy in women (Warrier et al., 2017), and deletion of this locus has been implicated in autism (Gunnarsson and Foyn Bruun, 2010; Pinto et al., 2014).

Because rats and mice were shown to be capable of learning from others, observational learning studies served as a foundation for studying empathy in rodents. However, observational learning occurs when the observer's task performance changes by observing the demonstrator, not necessarily sharing emotions, such as in foraging (Galef and Giraldeau, 2001). By contrast, emotional empathy occurs when the observer's emotional state changes in response to an expression of a similar emotion by a conspecific (de Waal and Preston, 2017; Panksepp and Lahvis, 2011). This phenomenon, referred to as emotional state-matching or affect sharing, was measured as socially transmitted fear response (vicarious freezing) in our behavioral paradigm. Importantly, we and others have provided evidence that the vicarious freezing response of the observer mouse was positively influenced by the animal's familiarity or kinship with the demonstrator. In other words, the demonstrator, being a sibling or long-time mating partner, tends to trigger a higher fear response in the observer (Gonzalez-Liencres et al., 2014; Jeon et al., 2010; Pisansky et al., 2017; Watanabe, 2011), a phenomenon similar to empathy in humans (Olsson et al., 2007). Further supporting this idea is a recent study showing that oxytocin, known as a distinct biological factor implicated in empathy-related behaviors in rodents and humans, increased neuronal activity within the ACC and enhanced observational fear in mice (Pisansky et al., 2017).

Because both the demonstrator and the observer mice contemporaneously express freezing response, one might consider that the freezing response in observational fear conditioning represents emotional contagion. However, when the observer mouse was placed alone back in the same chamber next day, the mouse showed a freezing response (contextual fear memory), although the observer had never experienced foot shocks. This indicates that an association has been made between the affective experience of the observer and the specific environment where the event happened. This subsequent effect should be distinct from emotional contagion or mimicry because this freezing behavior takes place in the absence of the demonstrator long after its exposure to the demonstrator. Because emotional empathy is broadly defined as emotional state-matching between individuals, the observational fear paradigm we study could be reasonably matched to affective empathy in humans (Debiec and Olsson, 2017; Meyza et al., 2017; Sivaselvachandran et al., 2016). In line with our view, "observational fear," "vicarious fear learning," "social fear learning," "empathic fear," and "empathy" have often been interchangeably used in recent work for rodent models of empathy (Atsak et al., 2011; Debiec and Olsson, 2017; Gonzalez-Liencres et al., 2014; Pisansky et al., 2017; Sanders et al., 2013; Watanabe, 2011).

The ACC has been implicated in fundamental cognitive processes, including executive processing, attention, affective emotion, and social cognition (Apps et al., 2016; Hutchison et al., 1999; Singer et al., 2004). The converging evidence of behavioral and neural mechanisms underlying observational fear highlights the ACC in association with the amygdala (Debiec and Olsson, 2017; Jeon et al., 2010). We have previously demonstrated that ACC activities are augmented and synchronized with those of the lateral amygdala (LA) during observational fear (Jeon et al., 2010), suggesting that the ACC encodes the affective and cognitive information required to express social fear. In the cortex, inhibitory neurons not only regulate excitatory-inhibitory balance in networks but also mediate the precise gating of information through specific signaling pathways (Kubota et al., 2016; Tremblay et al., 2016). In this study, we found that observational fear was enhanced by decreasing the inhibition of ACC pyramidal neurons via optogenetic suppression of SST+ neurons and impaired by activation of SST+ neurons. By contrast, decreasing inhibition of pyramidal neurons via optogenetic suppression of PV+ neurons or PV-specific *Nrxn3* deletion did not change the behavior. This suggests that SST+ neuron-specific mechanisms, not just any inhibition, control empathic fear responses. For optogenetic suppression, SST+ neurons in the right ACC were continuously photo-inhibited during the entire 4-min conditioning period, but this increased the level of vicarious freezing only in the first minute of the conditioning period (min 6). Because dendrite-targeting SST+ neurons exert distal inhibition to control incoming inputs to pyramidal neurons, our results suggest that silencing SST+ neurons enhanced observational fear by decreasing the inhibition of ACC pyramidal neurons. However, recent studies identified that there are different subtypes of SST+ neurons showing a layer-specific distinct disinhibition on pyramidal neurons and other inhibitory neurons in the cortex (Muñoz et al., 2017; Urban-Ciecko and Barth, 2016). Specifically, suppression of SST+ neurons in L2/3 increases the firing rates of nearby pyramidal neurons, whereas, in deeper layers, SST+ neurons inhibit PV+ neurons (Cottam et al., 2013; Gentet et al., 2012; Xu et al., 2013). It is possible that the net effect of silencing SST+ neurons in other layers is an increase in overall inhibition through PV+ neurons. Thus, we cannot exclude the possibility that our 4-min continuous optic inhibition caused some secondary compensatory effect after the transient effect in the early phase of conditioning. Nonetheless, our data showed that different types of cortical GABAergic neurons behaved differently and that SST+ neurons in the ACC bidirectionally controlled the degree of observational fear response. Similarly, inactivation of SST+ neurons increased the activity of hippocampal CA1 pyramidal cells and reduced contextual fear learning, whereas suppression of PV+ neurons had no effect on behavior (Lovett-Barron et al., 2014).

Our study demonstrates that the *Nrxn3*-mediated inhibitory function in SST+ interneurons in the ACC is a crucial neural mechanism for controlling the degree of socially transmitted fear. Given the similarity in neocortical circuit organization across brain areas and species (Harris and Shepherd, 2015; Tremblay et al., 2016), we propose that this inhibitory circuit motif mediated by SST+ neurons in the ACC may represent an effective and widely used neural mechanism controlling other empathy-related behaviors. Thus, it will be of great interest to determine whether *Nrxn3*-dependent SST+ neurons control other types of socially contagious behaviors, such as empathy for pain, consolation, or prosocial helping behaviors (Ben-Ami Bartal et al., 2011; Burkett et al., 2016; Langford et al., 2006). Furthermore, because cortical SST+ interneurons can be further subdivided into multiple subsets (Paul et al., 2017; Tasic et al., 2016; Zeng and Sanes, 2017), a more detailed cell type-specific genetic dissection of *Nrxn3* could help elucidate a distinct neuronal subpopulation-mediated circuit regulating empathy-related behaviors.

STAR★METHODS

Detailed methods are provided in the online version of this paper and include the following:

- KEY RESOURCES TABLE
- CONTACT FOR REAGENT AND RESOURCE SHARING
- EXPERIMENTAL MODEL AND SUBJECT DETAILS
- METHOD DETAILS
  - Whole-genome sequencing
  - PCR and DNA sequencing
  - Production of knock-in Nrxn3^{R498W} mice by CRISPR/-Cas9 technology
  - RNA extraction and TaqMan gene expression assay
  - Behavioral assays
  - Constructs
  - Viral injections and *in vivo* surgery
  - Optogenetic stimulations
  - Slice patch-clamp recording
  - Histology
- QUANTIFICATION AND STATISTICAL ANALYSIS
- DATA AND SOFTWARE AVAILABILITY

SUPPLEMENTAL INFORMATION

Supplemental Information includes seven figures, three tables, and five videos and can be found with this article online at https://doi.org/10.1016/j.neuron.2018.03.041.

ACKNOWLEDGMENTS

We thank J. Lee, J. Park, and C.F. Latchoumane for methodological advice and helpful discussions; B. Lee for designing a fDIO-Cre viral construct; Y. Jang for IVF; and Z.J. Huang (Cold Spring Harbor Laboratory) for providing SST-Flp mice. This work was supported by Institute for Basic Science (IBS) grant IBS-R001-D1, Republic of Korea.

AUTHOR CONTRIBUTIONS

S.K., A.K., and H.-S.S. conceived the project and designed all experiments. S.K. and A.K. performed all behavioral assays, WGS bioinformatics analyses, surgeries, and optogenetic experiments. J.J.S. and J.P. designed and performed the *ex vivo* electrophysiological recordings. J.-H.K. performed the histology experiments. S.K., A.K., and H.-S.S. wrote the manuscript.

DECLARATION OF INTERESTS

The authors declare no competing interests.

Received: December 4, 2017
Revised: February 19, 2018
Accepted: March 22, 2018
Published: April 19, 2018

REFERENCES

Aoto, J., Martinelli, D.C., Malenka, R.C., Tabuchi, K., and Südhof, T.C. (2013). Presynaptic neurexin-3 alternative splicing trans-synaptically controls postsynaptic AMPA receptor trafficking. Cell *154*, 75–88.

Aoto, J., Földy, C., Ilcus, S.M., Tabuchi, K., and Südhof, T.C. (2015). Distinct circuit-dependent functions of presynaptic neurexin-3 at GABAergic and glutamatergic synapses. Nat. Neurosci. *18*, 997–1007.

Apps, M.A., Rushworth, M.F., and Chang, S.W. (2016). The Anterior Cingulate Gyrus and Social Cognition: Tracking the Motivation of Others. Neuron *90*, 692–707.

Atsak, P., Orre, M., Bakker, P., Cerliani, L., Roozendaal, B., Gazzola, V., Moita, M., and Keysers, C. (2011). Experience modulates vicarious freezing in rats: a model for empathy. PLoS ONE *6*, e21855.

Baron-Cohen, S., and Wheelwright, S. (2004). The empathy quotient: an investigation of adults with Asperger syndrome or high functioning autism, and normal sex differences. J. Autism Dev. Disord. *34*, 163–175.

Ben-Ami Bartal, I., Decety, J., and Mason, P. (2011). Empathy and pro-social behavior in rats. Science *334*, 1427–1430.

Bernhardt, B.C., and Singer, T. (2012). The neural basis of empathy. Annu. Rev. Neurosci. *35*, 1–23.

Bernhardt, B.C., Valk, S.L., Silani, G., Bird, G., Frith, U., and Singer, T. (2014). Selective disruption of sociocognitive structural brain networks in autism and alexithymia. Cereb. Cortex *24*, 3258–3267.

Bird, G., Silani, G., Brindley, R., White, S., Frith, U., and Singer, T. (2010). Empathic brain responses in insula are modulated by levels of alexithymia but not autism. Brain *133*, 1515–1525.

Bora, E., Gökçen, S., and Veznedaroglu, B. (2008). Empathic abilities in people with schizophrenia. Psychiatry Res. *160*, 23–29.

Burkett, J.P., Andari, E., Johnson, Z.V., Curry, D.C., de Waal, F.B., and Young, L.J. (2016). Oxytocin-dependent consolation behavior in rodents. Science *351*, 375–378.

Camp, M., Norcross, M., Whittle, N., Feyder, M., D'Hanis, W., Yilmazer-Hanke, D., Singewald, N., and Holmes, A. (2009). Impaired Pavlovian fear extinction is a common phenotype across genetic lineages of the 129 inbred mouse strain. Genes Brain Behav. *8*, 744–752.

Camp, M.C., Macpherson, K.P., Lederle, L., Graybeal, C., Gaburro, S., Debrouse, L.M., Ihne, J.L., Bravo, J.A., O'Connor, R.M., Ciocchi, S., et al. (2012). Genetic strain differences in learned fear inhibition associated with variation in neuroendocrine, autonomic, and amygdala dendritic phenotypes. Neuropsychopharmacology *37*, 1534–1547.

Chen, Q., Panksepp, J.B., and Lahvis, G.P. (2009). Empathy is moderated by genetic background in mice. PLoS ONE *4*, e4387.

Chen, F., Venugopal, V., Murray, B., and Rudenko, G. (2011). The structure of neurexin 1α reveals features promoting a role as synaptic organizer. Structure *19*, 779–789.

Chen, L.Y., Jiang, M., Zhang, B., Gokce, O., and Südhof, T.C. (2017). Conditional deletion of all neurexins defines diversity of essential synaptic organizer functions for neurexins. Neuron *94*, 611–625.e4.

Chiu, C.Q., Lur, G., Morse, T.M., Carnevale, N.T., Ellis-Davies, G.C., and Higley, M.J. (2013). Compartmentalization of GABAergic inhibition by dendritic spines. Science *340*, 759–762.

Choi, Y., Sims, G.E., Murphy, S., Miller, J.R., and Chan, A.P. (2012). Predicting the functional effect of amino acid substitutions and indels. PLoS ONE *7*, e46688.

Church, R.M. (1959). Emotional reactions of rats to the pain of others. J. Comp. Physiol. Psychol. *52*, 132–134.

Cong, L., Ran, F.A., Cox, D., Lin, S., Barretto, R., Habib, N., Hsu, P.D., Wu, X., Jiang, W., Marraffini, L.A., and Zhang, F. (2013). Multiplex genome engineering using CRISPR/Cas systems. Science *339*, 819–823.

Cottam, J.C., Smith, S.L., and Häusser, M. (2013). Target-specific effects of somatostatin-expressing interneurons on neocortical visual processing. J. Neurosci. *33*, 19567–19578.

Courchesne, E., and Pierce, K. (2005). Why the frontal cortex in autism might be talking only to itself: local over-connectivity but long-distance disconnection. Curr. Opin. Neurobiol. *15*, 225–230.

de Waal, F.B. (2008). Putting the altruism back into altruism: the evolution of empathy. Annu. Rev. Psychol. *59*, 279–300.

de Waal, F.B.M., and Preston, S.D. (2017). Mammalian empathy: behavioural manifestations and neural basis. Nat. Rev. Neurosci. *18*, 498–509.

Debiec, J., and Olsson, A. (2017). Social Fear Learning: from Animal Models to Human Function. Trends Cogn. Sci. *21*, 546–555.

Decety, J. (2011). The neuroevolution of empathy. Ann. N Y Acad. Sci. *1231*, 35–45.

Dumitriu, D., Cossart, R., Huang, J., and Yuste, R. (2007). Correlation between axonal morphologies and synaptic input kinetics of interneurons from mouse visual cortex. Cereb. Cortex *17*, 81–91.

Ebstein, R.P., Israel, S., Chew, S.H., Zhong, S., and Knafo, A. (2010). Genetics of human social behavior. Neuron *65*, 831–844.

Festing, M.F., Simpson, E.M., Davisson, M.T., and Mobraaten, L.E. (1999). Revised nomenclature for strain 129 mice. Mamm. Genome *10*, 836.

Fuccillo, M.V., Földy, C., Gökce, Ö., Rothwell, P.E., Sun, G.L., Malenka, R.C., and Südhof, T.C. (2015). Single-Cell mRNA Profiling Reveals Cell-Type-Specific Expression of Neurexin Isoforms. Neuron *87*, 326–340.

Galef, B.G., Jr., and Giraldeau, L.A. (2001). Social influences on foraging in vertebrates: causal mechanisms and adaptive functions. Anim. Behav. *61*, 3–15.

Gentet, L.J., Kremer, Y., Taniguchi, H., Huang, Z.J., Staiger, J.F., and Petersen, C.C. (2012). Unique functional properties of somatostatin-expressing GABAergic neurons in mouse barrel cortex. Nat. Neurosci. *15*, 607–612.

Gonzalez-Liencres, C., Juckel, G., Tas, C., Friebe, A., and Brüne, M. (2014). Emotional contagion in mice: the role of familiarity. Behav. Brain Res. *263*, 16–21.

Gorski, J.A., Talley, T., Qiu, M., Puelles, L., Rubenstein, J.L., and Jones, K.R. (2002). Cortical excitatory neurons and glia, but not GABAergic neurons, are produced in the Emx1-expressing lineage. J. Neurosci. *22*, 6309–6314.

Gunnarsson, C., and Foyn Bruun, C. (2010). Molecular characterization and clinical features of a patient with an interstitial deletion of 3p25.3-p26.1. Am. J. Med. Genet. A. *152A*, 3110–3114.

Haaker, J., Golkar, A., Selbing, I., and Olsson, A. (2017). Assessment of social transmission of threats in humans using observational fear conditioning. Nat. Protoc. *12*, 1378–1386.

Hahamy, A., Behrmann, M., and Malach, R. (2015). The idiosyncratic brain: distortion of spontaneous connectivity patterns in autism spectrum disorder. Nat. Neurosci. *18*, 302–309.

Harris, K.D., and Shepherd, G.M. (2015). The neocortical circuit: themes and variations. Nat. Neurosci. *18*, 170–181.

Hefner, K., Whittle, N., Juhasz, J., Norcross, M., Karlsson, R.M., Saksida, L.M., Bussey, T.J., Singewald, N., and Holmes, A. (2008). Impaired fear extinction learning and cortico-amygdala circuit abnormalities in a common genetic mouse strain. J. Neurosci. *28*, 8074–8085.

Hermann, M., Stillhard, P., Wildner, H., Seruggia, D., Kapp, V., Sánchez-Iranzo, H., Mercader, N., Montoliu, L., Zeilhofer, H.U., and Pelczar, P. (2014). Binary recombinase systems for high-resolution conditional mutagenesis. Nucleic Acids Res. *42*, 3894–3907.

Hippenmeyer, S., Vrieseling, E., Sigrist, M., Portmann, T., Laengle, C., Ladle, D.R., and Arber, S. (2005). A developmental switch in the response of DRG neurons to ETS transcription factor signaling. PLoS Biol. *3*, e159.

Hutchison, W.D., Davis, K.D., Lozano, A.M., Tasker, R.R., and Dostrovsky, J.O. (1999). Pain-related neurons in the human cingulate cortex. Nat. Neurosci. *2*, 403–405.

Jeon, D., and Shin, H.S. (2011). A mouse model for observational fear learning and the empathetic response. Curr. Protoc. Neurosci., Chapter 8, Unit 8.27.

Jeon, D., Kim, S., Chetana, M., Jo, D., Ruley, H.E., Lin, S.Y., Rabah, D., Kinet, J.P., and Shin, H.S. (2010). Observational fear learning involves affective pain system and Cav1.2 Ca2+ channels in ACC. Nat. Neurosci. *13*, 482–488.

Keane, T.M., Goodstadt, L., Danecek, P., White, M.A., Wong, K., Yalcin, B., Heger, A., Agam, A., Slater, G., Goodson, M., et al. (2011). Mouse genomic variation and its effect on phenotypes and gene regulation. Nature *477*, 289–294.

Keum, S., and Shin, H.S. (2016). Rodent models for studying empathy. Neurobiol. Learn. Mem. *135*, 22–26.

Keum, S., Park, J., Kim, A., Park, J., Kim, K.K., Jeong, J., and Shin, H.S. (2016). Variability in empathic fear response among 11 inbred strains of mice. Genes Brain Behav. *15*, 231–242.

Kim, S., Mátyás, F., Lee, S., Acsády, L., and Shin, H.S. (2012). Lateralization of observational fear learning at the cortical but not thalamic level in mice. Proc. Natl. Acad. Sci. USA *109*, 15497–15501.

Kleberg, J.L., Selbing, I., Lundqvist, D., Hofvander, B., and Olsson, A. (2015). Spontaneous eye movements and trait empathy predict vicarious learning of fear. Int. J. Psychophysiol. *98*, 577–583.

Knafo, A., Zahn-Waxler, C., Davidov, M., Van Hulle, C., Robinson, J.L., and Rhee, S.H. (2009). Empathy in early childhood: genetic, environmental, and affective contributions. Ann. N Y Acad. Sci. *1167*, 103–114.

Kubota, Y., Karube, F., Nomura, M., and Kawaguchi, Y. (2016). The Diversity of Cortical Inhibitory Synapses. Front. Neural Circuits *10*, 27.

Langford, D.J., Crager, S.E., Shehzad, Z., Smith, S.B., Sotocinal, S.G., Levenstadt, J.S., Chanda, M.L., Levitin, D.J., and Mogil, J.S. (2006). Social modulation of pain as evidence for empathy in mice. Science *312*, 1967–1970.

Lovett-Barron, M., Turi, G.F., Kaifosh, P., Lee, P.H., Bolze, F., Sun, X.H., Nicoud, J.F., Zemelman, B.V., Sternson, S.M., and Losonczy, A. (2012). Regulation of neuronal input transformations by tunable dendritic inhibition. Nat. Neurosci. *15*, 423–430, S1–S3.

Lovett-Barron, M., Kaifosh, P., Kheirbek, M.A., Danielson, N., Zaremba, J.D., Reardon, T.R., Turi, G.F., Hen, R., Zemelman, B.V., and Losonczy, A. (2014). Dendritic inhibition in the hippocampus supports fear learning. Science *343*, 857–863.

Madisen, L., Zwingman, T.A., Sunkin, S.M., Oh, S.W., Zariwala, H.A., Gu, H., Ng, L.L., Palmiter, R.D., Hawrylycz, M.J., Jones, A.R., et al. (2010). A robust and high-throughput Cre reporting and characterization system for the whole mouse brain. Nat. Neurosci. *13*, 133–140.

Markram, H., Rinaldi, T., and Markram, K. (2007). The intense world syndrome–an alternative hypothesis for autism. Front. Neurosci. *1*, 77–96.

McLaren, W., Pritchard, B., Rios, D., Chen, Y., Flicek, P., and Cunningham, F. (2010). Deriving the consequences of genomic variants with the Ensembl API and SNP Effect Predictor. Bioinformatics *26*, 2069–2070.

Meyza, K.Z., Bartal, I.B., Monfils, M.H., Panksepp, J.B., and Knapska, E. (2017). The roots of empathy: Through the lens of rodent models. Neurosci. Biobehav. Rev. *76* (Pt B), 216–234.

Miller, M.T., Mileni, M., Comoletti, D., Stevens, R.C., Harel, M., and Taylor, P. (2011). The crystal structure of the α-neurexin-1 extracellular region reveals a hinge point for mediating synaptic adhesion and function. Structure *19*, 767–778.

Missler, M., Hammer, R.E., and Südhof, T.C. (1998). Neurexophilin binding to alpha-neurexins. A single LNS domain functions as an independently folding ligand-binding unit. J. Biol. Chem. *273*, 34716–34723.

Mizuno, S., Dinh, T.T., Kato, K., Mizuno-Iijima, S., Tanimoto, Y., Daitoku, Y., Hoshino, Y., Ikawa, M., Takahashi, S., Sugiyama, F., and Yagami, K. (2014). Simple generation of albino C57BL/6J mice with G291T mutation in the tyrosinase gene by the CRISPR/Cas9 system. Mamm. Genome *25*, 327–334.

Muñoz, W., Tremblay, R., Levenstein, D., and Rudy, B. (2017). Layer-specific modulation of neocortical dendritic inhibition during active wakefulness. Science *355*, 954–959.

Ng, P.C., and Henikoff, S. (2003). SIFT: Predicting amino acid changes that affect protein function. Nucleic Acids Res. *31*, 3812–3814.

Olsson, A., and Phelps, E.A. (2007). Social learning of fear. Nat. Neurosci. *10*, 1095–1102.

Olsson, A., Nearing, K.I., and Phelps, E.A. (2007). Learning fears by observing others: the neural systems of social fear transmission. Soc. Cogn. Affect. Neurosci. *2*, 3–11.

Panksepp, J.B., and Lahvis, G.P. (2011). Rodent empathy and affective neuroscience. Neurosci. Biobehav. Rev. *35*, 1864–1875.

Panksepp, J., and Panksepp, J.B. (2013). Toward a cross-species understanding of empathy. Trends Neurosci. *36*, 489–496.

Paul, A., Crow, M., Raudales, R., He, M., Gillis, J., and Huang, Z.J. (2017). Transcriptional architecture of synaptic communication delineates GABAergic neuron identity. Cell *171*, 522–539.e20.

Peterson, C. (2014). Theory of mind understanding and empathic behavior in children with autism spectrum disorders. Int. J. Dev. Neurosci. *39*, 16–21.

Pinto, D., Delaby, E., Merico, D., Barbosa, M., Merikangas, A., Klei, L., Thiruvahindrapuram, B., Xu, X., Ziman, R., Wang, Z., et al. (2014). Convergence of genes and cellular pathways dysregulated in autism spectrum disorders. Am. J. Hum. Genet. *94*, 677–694.

Pisansky, M.T., Hanson, L.R., Gottesman, I.I., and Gewirtz, J.C. (2017). Oxytocin enhances observational fear in mice. Nat. Commun. *8*, 2102.

Reissner, C., Runkel, F., and Missler, M. (2013). Neurexins. Genome Biol. *14*, 213.

Rodrigues, S.M., Saslow, L.R., Garcia, N., John, O.P., and Keltner, D. (2009). Oxytocin receptor genetic variation relates to empathy and stress reactivity in humans. Proc. Natl. Acad. Sci. USA *106*, 21437–21441.

Royer, S., Zemelman, B.V., Losonczy, A., Kim, J., Chance, F., Magee, J.C., and Buzsáki, G. (2012). Control of timing, rate and bursts of hippocampal place cells by dendritic and somatic inhibition. Nat. Neurosci. *15*, 769–775.

Sahin, M., and Sur, M. (2015). Genes, circuits, and precision therapies for autism and related neurodevelopmental disorders. Science *350*, aab3897.

Sanders, J., Mayford, M., and Jeste, D. (2013). Empathic fear responses in mice are triggered by recognition of a shared experience. PLoS ONE *8*, e74609.

Schreiner, D., Nguyen, T.M., Russo, G., Heber, S., Patrignani, A., Ahrné, E., and Scheiffele, P. (2014). Targeted combinatorial alternative splicing generates brain region-specific repertoires of neurexins. Neuron *84*, 386–398.

Simpson, E.M., Linder, C.C., Sargent, E.E., Davisson, M.T., Mobraaten, L.E., and Sharp, J.J. (1997). Genetic variation among 129 substrains and its importance for targeted mutagenesis in mice. Nat. Genet. *16*, 19–27.

Singer, T., Seymour, B., O'Doherty, J., Kaube, H., Dolan, R.J., and Frith, C.D. (2004). Empathy for pain involves the affective but not sensory components of pain. Science *303*, 1157–1162.

Sivaselvachandran, S., Acland, E.L., Abdallah, S., and Martin, L.J. (2016). Behavioral and mechanistic insight into rodent empathy. Neurosci. Biobehav. Rev., S0149-7634(16)30063-X.

Südhof, T.C. (2008). Neuroligins and neurexins link synaptic function to cognitive disease. Nature *455*, 903–911.

Südhof, T.C. (2017). Synaptic Neurexin Complexes: A Molecular Code for the Logic of Neural Circuits. Cell *171*, 745–769.

Sugita, S., Saito, F., Tang, J., Satz, J., Campbell, K., and Südhof, T.C. (2001). A stoichiometric complex of neurexins and dystroglycan in brain. J. Cell Biol. *154*, 435–445.

Taniguchi, H., He, M., Wu, P., Kim, S., Paik, R., Sugino, K., Kvitsiani, D., Fu, Y., Lu, J., Lin, Y., et al. (2011). A resource of Cre driver lines for genetic targeting of GABAergic neurons in cerebral cortex. Neuron *71*, 995–1013.

Tasic, B., Menon, V., Nguyen, T.N., Kim, T.K., Jarsky, T., Yao, Z., Levi, B., Gray, L.T., Sorensen, S.A., Dolbeare, T., et al. (2016). Adult mouse cortical cell taxonomy revealed by single cell transcriptomics. Nat. Neurosci. *19*, 335–346.

Tremblay, R., Lee, S., and Rudy, B. (2016). GABAergic Interneurons in the Neocortex: From Cellular Properties to Circuits. Neuron *91*, 260–292.

Treutlein, B., Gokce, O., Quake, S.R., and Südhof, T.C. (2014). Cartography of neurexin alternative splicing mapped by single-molecule long-read mRNA sequencing. Proc. Natl. Acad. Sci. USA *111*, E1291–E1299.

Ullrich, B., Ushkaryov, Y.A., and Südhof, T.C. (1995). Cartography of neurexins: more than 1000 isoforms generated by alternative splicing and expressed in distinct subsets of neurons. Neuron *14*, 497–507.

Urban-Ciecko, J., and Barth, A.L. (2016). Somatostatin-expressing neurons in cortical networks. Nat. Rev. Neurosci. *17*, 401–409.

Urban-Ciecko, J., Fanselow, E.E., and Barth, A.L. (2015). Neocortical somatostatin neurons reversibly silence excitatory transmission via GABAb receptors. Curr. Biol. *25*, 722–731.

Vaags, A.K., Lionel, A.C., Sato, D., Goodenberger, M., Stein, Q.P., Curran, S., Ogilvie, C., Ahn, J.W., Drmic, I., Senman, L., et al. (2012). Rare deletions at the neurexin 3 locus in autism spectrum disorder. Am. J. Hum. Genet. *90*, 133–141.

Vong, L., Ye, C., Yang, Z., Choi, B., Chua, S., Jr., and Lowell, B.B. (2011). Leptin action on GABAergic neurons prevents obesity and reduces inhibitory tone to POMC neurons. Neuron *71*, 142–154.

Warrier, V., Grasby, K.L., Uzefovsky, F., Toro, R., Smith, P., Chakrabarti, B., Khadake, J., Mawbey-Adamson, E., Litterman, N., Hottenga, J.J., et al. (2017). Genome-wide meta-analysis of cognitive empathy: heritability, and correlates with sex, neuropsychiatric conditions and cognition. Mol. Psychiatry. Published online June 6, 2017. https://doi.org/10.1038/mp.2017.122.

Watanabe, S. (2011). Empathy and reversed empathy of stress in mice. PLoS ONE *6*, e23357.

Wu, C., Orozco, C., Boyer, J., Leglise, M., Goodale, J., Batalov, S., Hodge, C.L., Haase, J., Janes, J., Huss, J.W., 3rd, and Su, A.I. (2009). BioGPS: an extensible and customizable portal for querying and organizing gene annotation resources. Genome Biol. *10*, R130.

Xu, H., Jeong, H.Y., Tremblay, R., and Rudy, B. (2013). Neocortical somatostatin-expressing GABAergic interneurons disinhibit the thalamorecipient layer 4. Neuron *77*, 155–167.

Yang, H., Wang, J.R., Didion, J.P., Buus, R.J., Bell, T.A., Welsh, C.E., Bonhomme, F., Yu, A.H., Nachman, M.W., Pialek, J., et al. (2011). Subspecific origin and haplotype diversity in the laboratory mouse. Nat. Genet. *43*, 648–655.

Yue, F., Cheng, Y., Breschi, A., Vierstra, J., Wu, W., Ryba, T., Sandstrom, R., Ma, Z., Davis, C., Pope, B.D., et al.; Mouse ENCODE Consortium (2014). A comparative encyclopedia of DNA elements in the mouse genome. Nature *515*, 355–364.

Zeng, H., and Sanes, J.R. (2017). Neuronal cell-type classification: challenges, opportunities and the path forward. Nat. Rev. Neurosci. *18*, 530–546.

STAR★METHODS

KEY RESOURCES TABLE

REAGENT or RESOURCE	SOURCE	IDENTIFIER
Antibodies		
mouse monoclonal anti-CRE	Millipore	MAB3120, RRID:AB_2085748
Alexa Fluor 488 donkey anti-mouse	Jackson ImmunoResearch Laboratories Inc.	Cat#715-545-150, RRID:AB_2340846
Bacterial and Virus Strains		
AAV9.EF1a.DIO.eNpHR3.0-eYFP.WPRE.hGH	Penn Vector Core	Cat#AV-9-26966P
AAV9.EF1a.DIO.ChETA(E123T/H134R)-eYFP.WPRE.hGH	Penn Vector Core	Cat#AV-9-26968P
AAV9.EF1a.DIO.eYFP.WPRE.hGH	Penn Vector Core	Cat#AV-9-27056
AAV9.EF1a.fDIO.Cre.WPRE	This paper, Penn Vector Core	N/A
AAV5-EF1a-fDIO-hChR2(H134R)-EYFP-WPRE	Karl Deisseroth, UNC Vector Core	Addgene#55639
AAV5.*Camk2α*.Cre.YFP	UNC Vector Core	N/A
AAV5.*Camk2α*.YFP	UNC Vector Core	N/A
Chemicals, Peptides, and Recombinant Proteins		
VECTASHIELD HardSet mounting medium with DAPI	Vector Laboratories	Cat#H-1500
Critical Commercial Assays		
TaqManGene Expression Assay	ThermoFisher Scientific	Mm01335648_m1/ABI(4448892) Nrxn3
Deposited Data		
The WGS data	NCBI Sequence Read Archive (https://submit.ncbi.nlm.nih.gov/)	SRP125244 and SRP124898
Experimental Models: Organisms/Strains		
Mouse: Emx1-IRES-Cre: B6.129S2-*Emx1*$^{tm1(cre)Krj}$/J	The Jackson Laboratory	JAX: 005628, RRID:IMSR_JAX:005628
Mouse: Vgat-IRES-Cre: *Slc32a1*$^{tm2(cre)Lowl}$/J	The Jackson Laboratory	JAX: 016962, RRID:IMSR_JAX:016962
Mouse: PV-IRES-Cre: B6;129P2-*Pvalb*$^{tm1(cre)Arbr}$/J	The Jackson Laboratory	JAX: 008069, RRID:IMSR_JAX:008069
Mouse: VIP-IRES-Cre: *Vip*$^{tm1(cre)Zjh}$/J	The Jackson Laboratory	JAX: 010908, RRID:IMSR_JAX:010908
Mouse: Ai14 Rosa26$^{LSL\text{-}tdT}$: B6.Cg-*Gt(ROSA)26Sor*$^{tm14(CAG\text{-}tdTomato)Hze}$/J	The Jackson Laboratory	JAX: 007914, RRID:IMSR_JAX:007914
Mouse: 129S2/SvPasCrl	Charles River Laboratories	Strain code: 476
Mouse: B6J. SST-IRES-Cre	Lovett-Barron et al., 2012 Royer et al., 2012	N/A
Mouse: SST-IRES-Flp: *Sst*$^{tm3.1(flpo)Zjh}$/J	Z. Josh Huang, Cold Spring Harbor Laboratory	JAX: 028579, RRID:IMSR_JAX:028579
Mouse: *Nrxn3*$^{f/f;}$ B6;129-*Nrxn3*^{tm3Sud}/J	The Jackson Laboratory	JAX: 014157, RRID:IMSR_JAX:014157
Oligonucleotides		
R498W genotyping primer	This paper	N/A
forward 5′-CCCAGTGAGTGATGGATTGATA-3′		
reverse 5′-GACAGGTGAGCATGCAAGTTAG-3′		
Nrxn3 floxed genotyping primer	The Jackson Laboratory	JAX: 014157
forward 5′-AATAGCAGAGGGGTGTGACAC-3′		
reverse 5′-CGTGGGGTATTTACGGATGAG-3′		
Recombinant DNA		
pCAG-Roxed-Cre	Hermann et al., 2014	Addgene#51273
pAAV-EF1a-fDIO-Cre-WPRE plasmid	This paper	N/A
Software and Algorithms		
SAMtools		http://samtools.sourceforge.net/
Ensembl Variant Effect Predictor (VEP)	McLaren et al., 2010	https://ensembl.org/Tools/VEP

(*Continued on next page*)

Continued		
REAGENT or RESOURCE	SOURCE	IDENTIFIER
Sorting Intolerant From Tolerant (SIFT)	Ng and Henikoff, 2003	https://ensembl.org/Tools/VEP
Protein Variation Effect Analyzer (PROVEAN) v1.1.3	Choi et al., 2012	http://provean.jcvi.org/protein_batch_submit.php?species=mouse
FreezeFrame	Coulbourn Instruments	Cat#ACT-100A
Genome Analysis Toolkit (GATK)	Broad Institute	https://software.broadinstitute.org/gatk
Clampex	Molecular Devices	N/A
Igor pro6.3	Wavemetrics	N/A
MiniAnalysis	Syanaptosoft	N/A
Digidata 1550A	Axon Instruments	N/A
Other		
NCBI Mouse ENCODE transcriptome	Yue et al., 2014	https://www.ncbi.nlm.nih.gov/gene/
Optic fibers 100 μm core, 0.22 NA, ZF 1.25, DFL	Doric Lenses Inc.	MFC_100/125-0.22_2.5_ZF1.25_DFL
Optical patch cord MFP_100/125/900-0.22_2m_FC-ZF1.25 with flange	Doric Lenses Inc.	MFP_100/125/900-0.22_2m_FC-ZF1.25(F)
Zirconia sleeves for optic fiber ferrules	Doric Lenses Inc.	SLEEVE_ZR_1.25
Yellow laser (561nm)	Changchun New Industries Optoelectronics Technology Corp.	Cat#MGL-FN-561
Blue laser (450nm)	Changchun New Industries Optoelectronics Technology Corp.	Cat#MDL-III-450
Multiclamp 700B	Axon Instruments	

CONTACT FOR REAGENT AND RESOURCE SHARING

Further information and requests for resources and reagents should be directed to and will be fulfilled by the Lead Contact, Hee-Sup Shin (shin@ibs.re.kr).

EXPERIMENTAL MODEL AND SUBJECT DETAILS

All inbred mouse strains, Emx1$^{tm1(cre)Krj}$ (Emx1-ires-Cre), Slc32a1$^{tm2(cre)Lowl}$ (Vgat-ires-Cre), Pvalb$^{tm1(cre)Arbr}$ (PV-ires-Cre), Vip$^{tm1(cre)Zjh}$ (VIP-ires-Cre), and Gt(ROSA)26Sor$^{tm14(CAG-tdTomato)Hze}$ (*Ai14* Rosa26$^{LSL-tdT}$) were obtained from The Jackson Laboratory and bred in-house for experiments. The 129S2/SvPas strain was obtained from the Charles River Laboratories. SST-ires-Cre mice were obtained from the Korean Institute for Science and Technology (Lovett-Barron et al., 2012; Royer et al., 2012) and SST-ires-Flp mice were kindly provided by Z. Josh Huang at Cold Spring Harbor Laboratory. All Cre mice were on a B6J background (> N10 back-cross). Conditional *Nrxn3*tm3Sud (*Nrxn3*$^{f/f}$) mice on a mixed genetic background were obtained from The Jackson Laboratory and bred with B6J strain for 5 generations before crossing with the Cre or Flp mice. All the animals were housed 2-5 animals per cage. Cages were maintained under 12/12-h light/dark cycle and at 23-25°C. Behavioral test rooms were at around 20°C. Food and water were available *ad libitum*. Male littermates were randomly assigned to either experimental or control group. Behavioral tests were done on visibly healthy (i.e., no skin irritation, agile, and no developmental malformation of eyes or teeth) mice in 10-14 weeks of age; electrophysiological slice experiments involving whole-cell patch clamp recordings were performed on P50-60 mice. All experiments were approved by the Institutional Animal Care and Use Committee of Institute for Basic Science (IBS).

METHOD DETAILS

Whole-genome sequencing

DNA sequencing and read alignment

High quality genomic DNA were extracted from the brains of two male 129S1 and two male 129S4 mice using a QIAGEN Genomic-tip 100/G kit. Genomic DNA was sheared to 200-300bp fragments using Covaris S2 and used to construct a sequencing library using the Illumina Truseq PCR free library construction tool according to the manufacturer's recommended protocol. The sequencing library prepared by random fragmentation of the DNA, followed by 5′ and 3′ adaptor ligation. Alternatively, "tagmentation" combines the fragmentation and ligation reactions into a single step that increases the efficiency of the library preparation process. Adaptor-ligated fragments are then PCR-amplified and gel-purified. For cluster generation, the library was loaded into a flow cell where fragments are captured on a lawn of surface-bound oligos complementary to the library adapters. Each fragment is then amplified into distinct, clonal clusters through bridge amplification. When cluster generation is complete, the templates are ready for sequencing using

Illumina HiSeq 2000 sequencer. As all 4 reversible, terminator-bound dNTPs are present during each sequencing cycle, natural competition minimizes incorporation bias and reduces raw error rates compared to other technologies. The result is highly accurate base-by-base sequencing that virtually eliminates sequence-context-specific errors, even within repetitive sequence regions and homopolymers. After sequencing, FastQC and quality filtering process was performed in order to reduce biases in the analysis. Filtered sequencing reads from each strain were aligned to the C57BL/6J mouse reference genome (GRCm38/mm10) using BWA aligner (with mem algorithm).

SNP and Indel discovery

The output, Sam file, was converted to Bam file and was sorted with SAMtools. PCR duplicate reads were removed with Picard tools. Statistics regarding this mapping result such as the number of reads and its coverage to all sequences was obtained using the Genome Analysis Toolkit (GATK). To ensure that high quality variants were only used for later analysis, variant calling was performed with SAMtools (mpileup command) and BCFtools (call, filter) commando on the basis of the BAM file previously generated). In this step, SNPs and short insertion or deletion (indel) candidates with phred scores over 30 (base call accuracy 99.9%) were captured through aligned reads' information. Only homozygote high quality variants that passed all the filters were retained. Those variants classified by chromosomes or scaffolds, and the information of the location are described in Supplemental information.

Identification and count of 129S1-unique variations

To identify variants unique to 129S1 strain, variants found in 129S1 strain that differ from those of 129S4 strain were then compared with 17 other inbred mouse strains in the Mouse Genome Project (MGP) variation catalog. We then filtered 129S1-unique variant sets (SNPs and indels) to identify potentially pathogenic variants.

SNP and indel annotation and prediction of consequences

Using the Ensembl Variant Effect Predictor (VEP) tool (McLaren et al., 2010), we added functional consequence annotation to SNPs and indels on gene transcripts. For missense variants, we employed "Sorting Intolerant From Tolerant (SIFT) (Ng and Henikoff, 2003) score estimated by the VEP to predict whether amino acid substitution would be damaging, and Protein Variation Effect Analyzer (PROVEAN) v1.1.3 (Choi et al., 2012) to provide further prediction of the functional effect of protein changes. To further narrow down the causative variants, we then compared the abundance of mRNA for the genes harboring 129S1-unique missense variants using the BioGPS (Wu et al., 2009) and the NCBI Mouse ENCODE transcriptome data (Yue et al., 2014).

PCR and DNA sequencing

Tail genomic DNA was isolated using chloroform extraction. The R498W variant-containing region in exon 6 of the *Nrxn3* gene was amplified using standard PCR conditions (94°C for 2min, 94°C for 30 s, 60°C for 30 s, 72°C for 30 s, 30 cycles). R498W primer sequences were as follows (636bp amplicon, Forward primer: 5′-CCCAGTGAGTGATGGATTGATA-3′, reverse primer: 5′-GACAGGT GAGCATGCAAGTTAG-3′; sequencing Primer, 5′-TGCAAGACTGATTCATATG 3′).

Production of knock-in Nrxn3^{R498W} mice by CRISPR/Cas9 technology

To produce a Cas9/single-guide RNA (sgRNA) expression vector, oligonucleotide DNAs (5′caccCGGACATCTTTCCTTTCTTG AGG-3′ and 5′-aaacCCTCAAGAAAGGAAAGATGTCCG-3′) were annealed and then inserted into pX330 vector (Addgene). The cleavage activity of the pX330-Nrxn3Ex6 vector was evaluated by the EGxxFP system as described previously (Cong et al., 2013; Mizuno et al., 2014). Genomic DNA containing exon 6 of the *Nrxn*3 gene was amplified and inserted into pCAG-EGxxFP to produce pCAG-EGxxFP-Nrxn3Ex6. The pX330-Nrxn3Ex6 and pCAG-EGxxFP-Nrxn3Ex6 were transfected into HEK293 cells (Laboratory Animal Resource Center, University of Tsukuba, Japan). As a donor oligonucleotide, a single-stranded nucleotide DNA was synthesized (Integrated DNA Technologies). Female C57BL/6J mice were injected with pregnant mare serum gonadotropin and human chorionic gonadotropin at a 48-h interval, and mated with male C57BL/6J mice. The fertilized one-cell embryos were collected from the oviducts. Then, 5 ng/μL of pX330-Nrxn3Ex6 vector and 10 ng/μL of the donor oligonucleotide were injected into the pronuclei of these one-cell-stage embryos. The injected one-cell embryos were then transferred into pseudopregnant ICR mice. The Trp^{498} coding change in F0 mice was confirmed by DNA sequencing of the PCR product for the exon 6 of the *Nrxn3* gene. A total of 112 mice of B6J background were born and three F0 mouse lines with the R498W coding variant were identified. Two founder mice containing indels were excluded and one F0 line harboring only the R498W variant was further examined for the presence of the Cas9 transgene and off-target effects. Candidate off-target sites were identified based on a complete match of 16 bp at the 3′ end, including the PAM sequence. F0 mice were backcrossed with C57BL/6J mice for two generations before intercrossing heterozygotes (KI-*Nrxn3*^{RW}) to generate homozygote mutant (KI-*Nrxn3*^{WW}) mice.

RNA extraction and TaqMan gene expression assay

Total RNA was extracted from frontal cortices of 129S1, 129S8, KI-*Nrxn3*^{RR}, and KI-*Nrxn3*^{WW} mice using RNeasy mini kit (QIAGEN, USA). Reverse transcription was performed on 1 μg of RNA using Superscript VILO reverse transcriptase (Invitrogen, USA). The relative abundance of *Nrxn3* mRNA transcript was assessed by TaqMan qRT-PCR (ThermoFisher Scientific, USA) using a standard curve method. Quantification of RT-PCR products were measured by examining the increase in emitted fluorescence signal from the FAM dye. All samples were run in triplicate and an additional assay for endogenous *Gapdh* gene was performed to control for input cDNA template quantity. Relative quantification was determined for each sample by calculating the mean Cq value using the delta Ct method.

Behavioral assays

All behavioral tests were performed at 2-7pm during the light cycle. Additionally, Day 2 contextual memory test was performed at a similar time of day as conditioning. Mice in their respective home cages were placed in the behavioral test room about an hour before the tests. Naive mice that had no prior experience on any behaviors were used only once for each of the behavioral assays. Each of the behavioral tests was performed as mice became available from breeding (at least 3 different litters), and in no particular order by strain or mutant line. Sample sizes were estimated based on previous studies using similar experimental designs (Jeon et al., 2010; Keum et al., 2016).

Observational fear

Observational fear conditioning was performed as previously described (Jeon and Shin, 2011). 10-12 weeks-old male mice (observer and demonstrator) were individually placed in chambers partitioned by a porous, transparent Plexiglas divider in the middle. After a 5 min habituation period, a 2 s foot shock (1 mA) was delivered every 10 s for 4 min to the demonstrator mouse. To assess contextual memory, the observer mice were placed back into the chamber 24 hr after training for 4 min. In all experiments, the observer and demonstrator mice were non-siblings and non-cagemates. The behavior of the mice was recorded with the Freezeframe software (Coulbourn Instruments) and analyzed with Freezeview software (Coulbourn Instruments). Motionless bouts lasting more than 1 s were considered as freeze.

Pavlovian fear conditioning

Conventional fear conditioning was performed as previously described (Jeon et al., 2010). On training day, mice were placed in the fear conditioning chamber (Coulbourn Instruments). After a 5 min exploration period, 3 foot shocks (0.7mA/ 1 s) separated by 1 min intervals were delivered to the mice. The mice remained in training chamber for another 60 s before being returned to home cages. To assess contextual learning, we placed the mice back into the chamber 24 hr after training. The behavior of the mice was recorded and analyzed with FreezeFrame software as described above.

Constructs

The pAAV-EF1a-fDIO-Cre-WPRE plasmid was constructed by replacing the 1,661 bp hChR2(H124R)-EYFP in AAV-EF1a-fDIO-hChR2(H134R)-EYFP-WPRE (a gift from Karl Deisseroth, Addgene # 55639) with a DNA fragment containing the 952 bp iCre flanked by BamHI and SacI sites in pCAG-Roxed-Cre (Addgene #51273) vector (Hermann et al., 2014). Adeno-associated viral (AAV) vectors were serotyped with AAV9 coat proteins and packaged by the University of Pennsylvania Vector Core (Penn vector core).

Viral injections and *in vivo* surgery

Adult mice were first put in a gas chamber (Vapormatic Ltd) filled with a mixture of isoflurane (4%) and oxygen (at 2L/min), and anesthetized with 8mg/mL ketamine (16% by volume) and xylazine (2.8% by volume) in saline solution intraperitoneally injected (0.015mL/g). Anesthetized mice were head-fixed on a stereotaxic equipment (Kopf Instruments). A heating pad ensured maintenance of core body temperature at 36°C. Antiseptics and lidocaine were applied before making incision on skin. Single or multiple cranial openings were made with dental drills, then a volume of about 0.5 μL virus solution was injected using pressure (Picospritzer III, Parker Hannifin Corp.) into the right ACC (AP/MD/DV, 1.0/0.3/1.5 mm). The injection glass pipette was then slowly removed after 10 min for diffusion. The optic fiber (Doric Lenses Inc., 100 μm core, 0.22 NA, ZF 1.25, DFL) was targeted to the same position as that used for the virus injection, dental cement was applied to cover the skull, and was allowed to harden for 10 min. Behavioral experiments were performed at least 3 weeks post-surgery. Cell-type-specific expression of virus was achieved using the following Cre-dependent AAV: AAV9-EF1a-DIO-eNpHR3.0-eYFP-WPRE-hGH (Penn vector core), AAV9-Ef1a-DIO-ChR (ChETA, E123T/H134R)-eYFP-WPRE-hGH (Penn vector core), or AAV5-*Camk2α*-Cre-YFP (UNC vector core). Control mice were injected with the following: AAV9-EF1a-DIO-eYFP-WPRE-hGH (Penn vector core), AAV5-*Camk2α*-YFP (UNC vector core), or AAV5-Ef1a-fDIO-ChR-EYFP (UNC vector core).

Optogenetic stimulations

Virus and optic fibers were stereotactically injected into the right ACC of mice at 7-8 weeks of age. 3-4 weeks after injection, each mouse was handled and attached toa dummy optical patch cord (Doric Lenses Inc., MFP_100/125/900-0.22_2m_FC-ZF1.25 with flange) with a zirconia sleeve (Doric Lenses Inc., SLEEVE_ZR_1.25) for habituation on cotton-gloved-hands for about 10 minutes each day for 3-5 days. Then, they were undergone observational fear conditioning under photostimulation, and contextual memory retrieval was measured 24 hours later, without attachment to an optical cable. Optic stimulation preceded by 1 s and continued throughout the 4 min observational fear conditioning. To perform optogenetic stimulation of NpHR and ChR2, we used diode-pumped solid state blue and yellow lasers with analog intensity control (MGL-FN-561 (yellow, 561nm) and MDL-III-450 (blue, 450nm), Changchun New Industries Optoelectronics Technology Corp.) The stimulation parameter are as follows. Yellow light: 241 s duration, continuous light, 0.9-1.4 mW at the tip of 100 μm optic fiber; blue light: 241 s duration, 20Hz, 5 ms pulse width, 0.5-1.0 mW at the fiber tip.

Slice patch-clamp recording

Animals were anesthetized with isoflurane and decapitated. Coronal slices of ACC (300μm) were prepared in sucrose-based cutting solution on Vibrating Microtome 7000smz-2 (Campden instruments, England), and recovered in sucrose-based cutting solution for

30min at 33-34°C. Slices were then transferred to a recording chamber perfused with oxygenated artificial cerebral spinal fluid (ACSF) at 32-35°C. Patch pipettes were pulled from borosilicate glass on a Flaming-Brown micropipette puller model P-1000 (Sutter Instruments, USA). Patch pipettes had a resistance of 4-6MΩ. Signals were recorded using a patch-clamp amplifier (Multiclamp 700B, Axon Instruments, USA) and digitized with Digidata 1550A (Axon Instruments, USA) using Clampex software. Signals were amplified, sampled at 10 kHz, and filtered to 2 or 5 kHz. Intrinsic excitability recording was performed on pyramidal neurons, identified by large apical dendrites, and SST+ neurons, identified by fluorescent tdTomato expression, and held in current clamp at −70mV. Action potentials (APs) were generated by injecting 500-ms-long current steps increasing by 50pA. APs were analyzed in Igor pro6.3 (Wavemetrics, USA). Miniature post-synaptic currents (mPSCs) were recorded in pyramidal neurons and SST+ interneurons with bath application of Tetrodotoxin (TTX), and analyzed in MiniAnalysis (Syanaptosoft, USA). All events in 5 min were averaged to determine mPSC area. Dual whole-cell patch recording was performed on pyramidal neuron, held in voltage clamp at 0mV for recording outward inhibitory post-synaptic currents (IPSC), and on SST+ neurons, held in current clamp at −70mV with single AP generation. To record possible axo-dendritic synaptic connection between SST+ (pre-) and pyramidal neurons (post-), current clamp recordings in SST+ neurons and voltage clamp recordings in pyramidal neurons were conducted simultaneously. Synaptic pairing was typically assessed by averaging 100 individual traces separated by 15 s. Presynaptic AP induced eIPSCs in pyramidal neurons at monosynaptic latencies (5.044msec ± 0.133) in all recorded pairs. Sucrose-based cutting solution (in mM): sucrose, 75; NaCl, 76; KCl, 2.5; $NaHCO_3$, 25; Glucose, 25; NaH_2PO_4,1.25; $MgSO_4$, 7; $CaCl_2$, 0.5; pH 7.3, and 310 mOsm. Standard ACSF (in mM) was NaCl, 124; KCl, 2.5; $MgCl_2$, 1.3; $CaCl_2$, 2.5; NaH_2PO_4, 1.0; $NaHCO_3$, 26.2; Glucose, 20; pH 7.4, 310 mOsm. Internal solution for intrinsic excitability (in mM) was K-gluconate, 135; NaCl, 7; HEPES, 10; EGTA, 0.5; Mg-ATP, 2; Na2-GTP, 0.3; Na-phosphocreatine, 10; pH 7.3, 295 mOsm. Internal solution for dual patch recording (in mM) was K-gluconate, 110; KCl, 30; HEPES, 10; EGTA, 0.5; Na-phosphocreatine, 10; Mg-ATP, 4; Na-GTP, 0.3; pH 7.3, 295 mOsm. Internal solution for mPSC recording (in mM) was CsMS, 135; CsCl, 10; HEPES, 10; EGTA, 0.2; Mg-ATP, 4; Na2-GTP, 0.4; pH 7.3, 295 mOsm.

Histology

After behavioral experiments, mice were undergone perfusion and fixation for examination of virus infection topography and position of optic fiber. Mice were intraperitoneally injected with about 0.8mL 2% Avertine in saline solution, and when they were fully anesthetized, transcardially infused with saline, then 4% paraformaldehyde (PFA) in 0.1M phosphate-buffered saline (PBS). Harvested brains were post-fixated in 4% PFA (< 4°C) overnight and the fixed brain was sectioned into in 50 μm coronal slices with a vibratome (Leica VT 1200S). fDIO-Cre- or *Camk2α*-Cre- injected samples were then blocked in 3% normal goat serum with 0.1% triton X (Sigma, T8787) in PBS (1hr, 25°C) before being stained with mouse monoclonal anti-CRE recombinase (1:400, Millipore, MAB3120) overnight (< 4°C). The slices were then incubated in Alexa Fluor 488 donkey anti-mouse (1:500, Jackson ImmunoResearch Labs) before being mounted on a glass slide with the Vectashield mounting medium (Vector Labs). The slides were imaged using a confocal microscope (Nikon eclipse Ti).

QUANTIFICATION AND STATISTICAL ANALYSIS

All the data presented indicate means ± s.e.m. Statistical analyses were performed in SigmaPlot 12 (Systat Software, Inc). Normality was assessed using Shapiro-Wilk tests. When the normality test failed, subject group analysis of non-parametric data was done with Kruskal–Wallis statistics followed by Dunn's multiple comparison test. No statistical methods were used to predetermine sample size. Variance in normally distributed datasets was analyzed with one-way or two-way analysis of variance (ANOVA) and Tukey's post hoc tests. Single variable comparisons were made with two-tailed Student's t tests. For *ex vivo* patch recording, statistical analysis of cumulative probabilities was tested by a Kolmogorov-Smirnov test from: http://www.physics.csbsju.edu/stats/KS-test.n.plot_form.html. Significance levels are indicated as follows:*$p < 0.05$; **$p < 0.01$; ***$p < 0.001$.

DATA AND SOFTWARE AVAILABILITY

The accession numbers for the whole genome sequence (WGS) of 129S1 and 129S4 mouse strains reported in this paper are NCBI SRA: SRP125244 and SRP124898.

Neuron, Volume *98*

Supplemental Information

A Missense Variant at the *Nrxn3* Locus Enhances Empathy Fear in the Mouse

Sehoon Keum, Arie Kim, Jae Jin Shin, Jong-Hyun Kim, Joomin Park, and Hee-Sup Shin

Supplemental Information

A Missense Variant at the *Nrxn3* Locus Enhances Empathy Fear in the Mouse

Sehoon Keum, Arie Kim, Jae Jin Shin, Jong-Hyun Kim, Joomin Park, Hee-Sup Shin

Supplemental Table 1

WGS	129S1	129S4
Total reads	1,137,141,158	898,093,236
Total yield (bp)	111,255,492,621	87,763,326,009
Read length (bp)	97.84	97.72
Reference length (non-N sites) (bp)	2,647,537,730	2,647,537,730
Initial mappable reads	1,099,309,337	881,964,588
% Initial mappable reads (out of total reads)	96.70%	98.20%
Mappable reads (remove duplicate)	942,069,507	830,387,261
Mappable yield (bp)	91,563,428,237	81,035,968,341
% Mappable reads (out of total reads)	82.80%	92.50%
% Coverage of regions (more than 1X)	99.60%	99.60%
Base coverage of regions (more than 1X)	2,637,096,522	2,635,876,684
% Coverage of regions (more than 10X)	97.50%	96.80%
Base coverage of regions (more than 10X)	2,580,342,982	2,561,997,323
Mean read depth (Mappable yield)	34.6	30.6
Number of SNPs	10,458,282	10,438,134
Number of coding SNPs	72,368	72,090
Number of synonymous SNPs	46,196	45,946
Number of nonsynonymous SNPs	25,406	25,372
Number of Indels	2,261,386	2,257,506
Number of coding Indels	1,122	1,138

Supplemental Table 1, Related to Figure 2 and STAR Methods. Whole-genome sequencing (WGS) coverage statistics of 129S1 and 129S4 strains.

Supplemental Table 2

A

Description	# number
UTR	74
ncRNA	176
Intronic	2404
Intergenic	1960
upstream& downstream	125
Synonymous	73
Non-Synonymous	**32**
SNPs in 129S1 different from 129S4	4,844

B

Gene	SNP	129S1	129S4	129S5	129P2	B6J (ref)	A/J	AKR	BALBc	C3H	B6N	CBA	DBA	FVB	LP	NOD	NZO	CAST	PWK	SPRET	WSB
Nrxn3	rs241832271	T	C	C	C	C	C	C	C	C	C	C	C	C	C	C	C	C	C	C	C
Myo7b	rs264343324	A	G	G	G	G	G	G	G	G	G	G	G	G	G	G	G	G	G	G	G
Olfr214	rs240242962	C	T	T	T	T	T	T	T	T	T	T	T	T	T	T	T	T	T	T	T
Nlrp10	rs253330544	T	G	G	G	G	G	G	G	G	G	G	G	G	G	G	G	G	G	G	G
Tmem120a	rs32247753	T	C	C	C	C	C	C	C	C	C	C	C	C	C	C	C	C	C	C	C
Rpl4	rs50793796	G	A	A	A	A	A	A	A	A	A	A	A	A	A	A	A	A	A	A	A
Lama4	rs51318920	A	C	C	C	C	C	C	C	C	C	C	C	C	C	C	C	C	C	C	C
Arvcf	rs32357197	A	G	G	G	G	G	G	G	G	G	G	G	G	G	G	G	G	G	G	G
Car9	rs226649018	G	A	G	A	A	A	A	A	A	A	A	A	A	A	A	A	G	G	G	G
Car9	rs229935653	A	G	A	G	G	G	G	G	G	G	G	G	G	G	G	G	G	G	G	A
Car9	rs230998527	A	G	A	G	G	G	G	G	G	G	G	G	G	G	G	G	G	G	G	A
Car9	rs27831237	A	G	A	G	G	G	G	G	G	G	G	G	G	G	G	G	G	G	G	G
Creb3	rs13459506	C	T	C	T	T	C	C	C	C	T	C	C	C	T	C	C	C	C	C	T
Creb3	rs32372405	C	G	C	G	G	G	C	G	G	G	G	G	G	G	C	C	C	C	C	G
Fam214b	rs3141921	A	G	A	G	G	G	G	G	G	G	G	G	G	G	G	G	G	G	G	G
Gba2	rs28327690	T	C	T	C	C	C	C	C	C	C	C	C	C	C	C	C	C	C	C	C
Hint2	rs218587352	A	G	A	G	G	G	G	G	G	G	G	G	G	G	G	G	G	G	G	G
Olfr70	rs31891745	T	C	T	C	C	T	T	T	T	C	C	C	C	C	T	C	T	T	T	C
Pigo	rs3147290	C	G	C	G	G	C	C	C	C	G	C	C	C	G	C	C	C	G	G	C
Prkdc	rs4164952	T	C	C	C	C	C	C	T	C	C	C	C	C	C	C	C	C	C	C	C
Reck	rs49467996	C	A	C	A	A	A	C	A	A	A	C	C	C	A	C	A	C	C	C	C
Rusc2	rs27850061	G	T	G	T	T	T	G	T	T	T	G	G	G	T	G	T	G	G	G	G
Rusc2	rs48111477	T	C	T	C	C	C	T	C	C	C	T	T	T	C	T	C	T	C	C	T
Rusc2	rs48608355	A	C	A	C	C	C	A	C	C	C	A	A	A	C	A	C	C	C	C	A
Rusc2	rs27850001	G	A	G	A	A	A	G	A	A	A	G	G	G	A	G	A	G	G	G	G
Rusc2	rs27864770	G	A	G	A	A	A	G	A	A	A	G	G	G	A	G	A	G	G	G	G
Rusc2	rs265461348	G	A	G	A	A	A	G	A	A	A	G	G	G	A	G	A	G	G	G	G
Rusc2	rs27864768	G	A	G	A	A	A	G	A	A	A	G	G	G	A	G	A	G	G	G	G
Spag8	rs28320598	T	C	T	C	C	T	T	T	T	C	C	C	C	C	T	C	T	T	T	C
Sytl2	rs50124233	G	A	A	G	A	A	A	A	A	A	A	A	G	A	A	A	A	A	A	A
Tesk1	rs233521879	A	G	A	G	G	G	G	G	G	G	G	G	G	G	G	G	G	G	G	G
Uts2b	rs51345000	G	T	T	T	T	T	T	T	G	T	G	G	T	G	T	G	G	G	G	G

Supplemental Table 2, Related to Figure 2. (**A**) Summary of the identified 129S1-unique SNPs different from those of 129S4 strain. **(B)** 32 non-synonymous coding SNPs identified in 129S1 strain compared with 19 inbred strains including 4 wild-derived strains (gray).

Supplemental Table 3

Gene symbol	Description	SNP	Protein change	Functional prediction		Brain Expression	
				SIFT	Provean	BioGPS	ENCODE
Nrxn3	Neurexin 3	rs241832271	R498W	Damaging	Deleterious	O	O
Tmem120a	transmembrane protein 120A	rs32247753	R249Q	Damaging	Deleterious	X	X
Myo7b	myosin VIIB	rs264343324	P2002S	Damaging	Deleterious	X	X
Olfr214	olfactory receptor 214	rs240242962	C249R	Damaging	Deleterious	N/A	N/A
Rpl4	ribosomal protein L4	rs50793796	T287A	Tolerated	Neutral	O	O
Lama4	laminin, alpha 4	rs51318920	S1111R	Tolerated	Neutral	O	O
Arvcf	armadillo repeat gene deleted in velo-cardio-facial syndrome	rs32357197	V462I	Tolerated	Neutral	O	O
Nlrp10	NLR family, pyrin domain containing 10	rs253330544	Q562K	Tolerated	Neutral	X	X

Supplemental Table 3, Related to Figure 2 and STAR Methods. Prioritization of the eight genes on the basis of predicted effect of the protein change and mRNA abundance in the brain.

Supplemental Figure 1

VARIATION		PROTEIN SEQUENCE CHANGE			
ROW_NO.	INPUT	PROTEIN_ID	POSITION	RESIDUE_REF	RESIDUE_ALT
1	ENSMUSP00000127407 498 R W	ENSMUSP00000127407	498	R	W

PROVEAN PREDICTION			
SCORE	PREDICTION (cutoff=-2.5)	#SEQ	#CLUSTER
-3.53	Deleterious	238	30

SIFT PREDICTION			
SCORE	PREDICTION (cutoff=0.05)	MEDIAN_INFO	#SEQ
0.002	Damaging	3.33	210

Supplemental Figure 1, Related to Figure 2. PROVEAN (Protein Variation Effect Analyzer) output indicates that the R498W variant in NRXN3 is considered deleterious.

Supplemental Figure 2

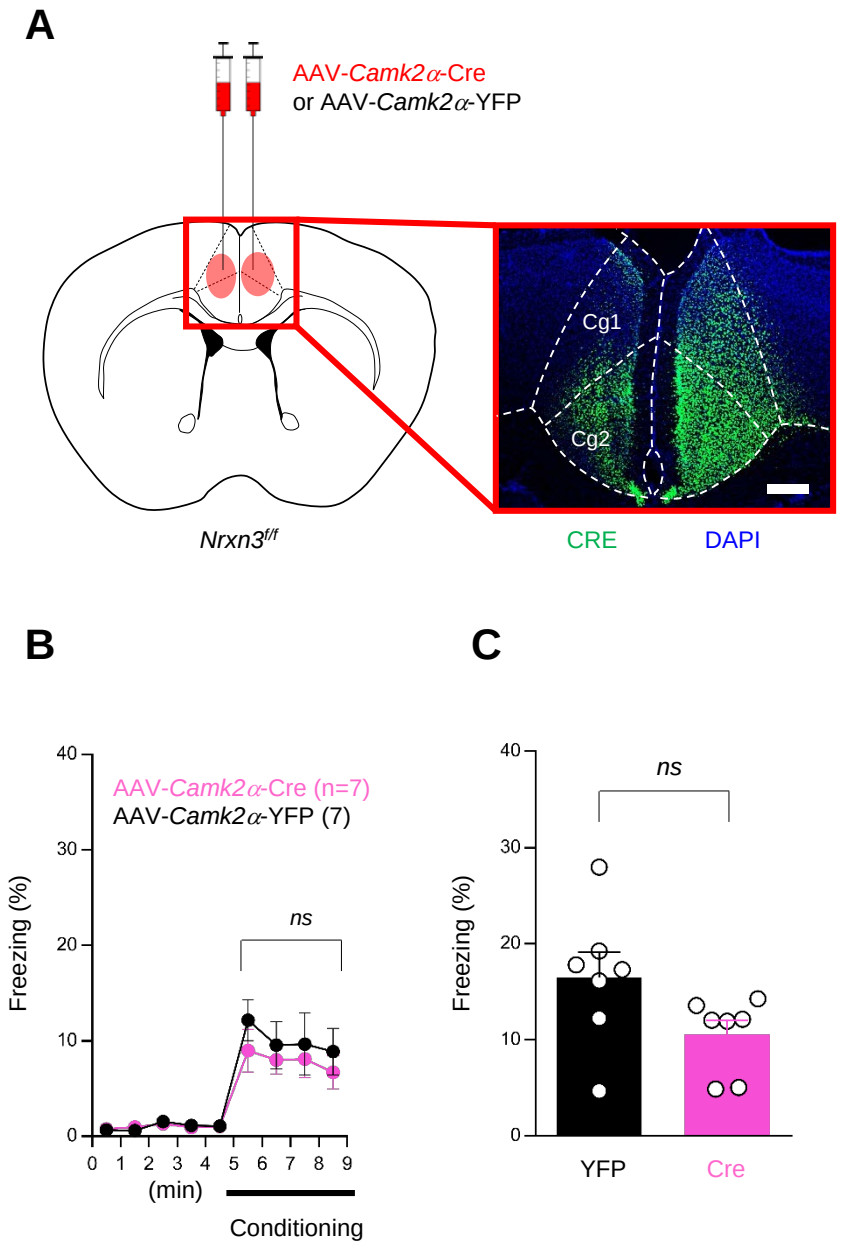

Supplemental Figure 2, Related to Figure 4. Observational fear in mice lacking *Nrxn3* in excitatory pyramidal neurons in the ACC. (**A**) Bilateral injection of AAV-*CamK2*α-Cre-YFP to selectively delete *Nrxn3* in putative excitatory pyramidal neurons (PNs) in the ACC, and a representative confocal image of the ACC of a *Nrxn3*$^{f/f}$ mouse (blue, DAPI; green, YFP). Cg, cingulate cortex. Bregma 1.0 mm rostral. Scale bar, 200µm. (**B,C**) Mice with PN-specific *Nrxn3* deletion (*n* =7) showed no difference in observational fear and 24hr retrieval as compared to control mice (*n* =7) with AAV-*CamK2*α-eYFP. All data are shown as mean ± s.e.m. *ns*, not significant.

Supplemental Figure 3

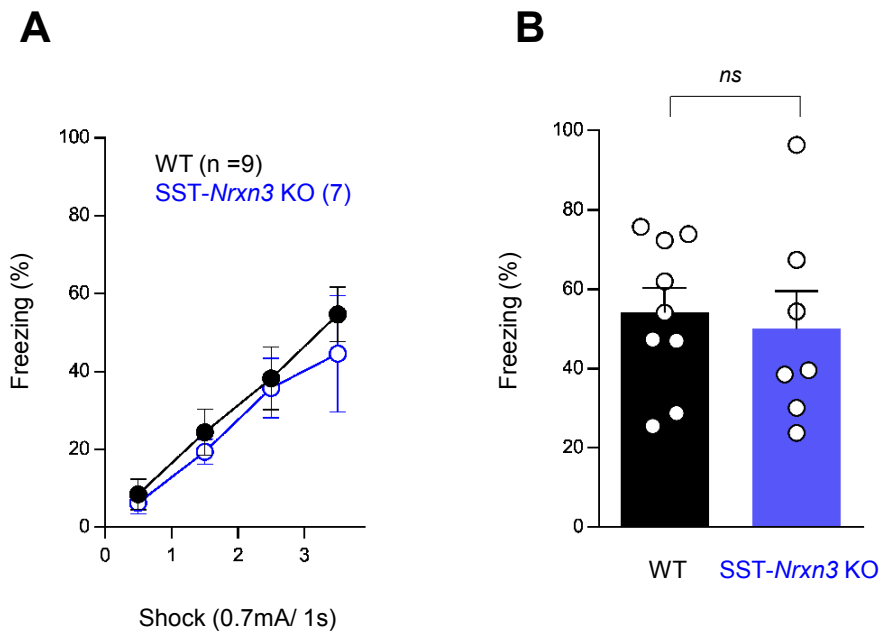

Supplemental Figure 3, Related to Figure 4. Classical fear conditioning in SST-*Nrxn3* KO mice. (**A**) SST-*Nrxn3* KO observer mice (*n* =7) show similar response in conditioned fear over trials as compared with WT littermate (*n* =9). (**B**) No difference in 24hr contextual fear memory between SST-*Nrxn3* KO and WT mice. All data are shown as mean ± s.e.m. *ns*, not significant.

Supplemental Figure 4

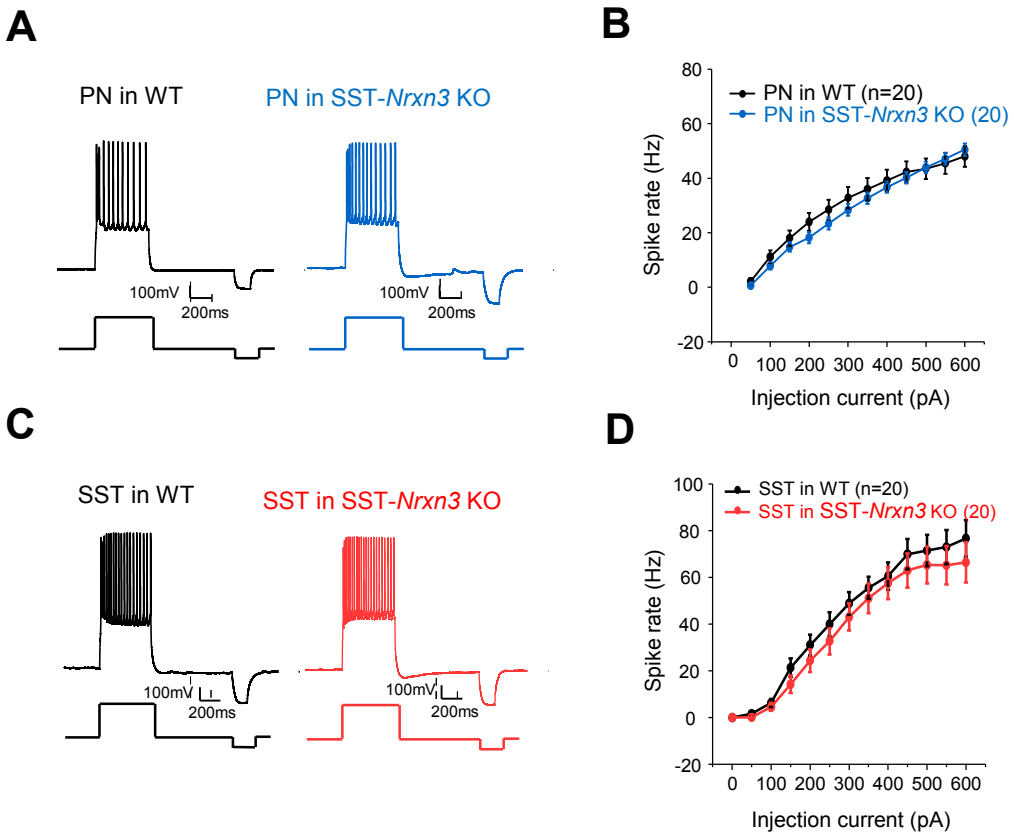

Supplemental Figure 4, Related to Figure 5. (**A**) Representative current-clamp recordings of APs generated by current injection (300 pA) in pyramidal neurons (PN) from WT (left, black) and SST-*Nrxn3* KO (right, blue) mice. (**B**) Input-output (IO) curve of averaged frequency of AP firing at different step current injections from PNs from WT (*n* =20, black) and SST-*Nrxn3* KO (*n* =20, blue) mice. (**C**) Representative current-clamp recordings from red fluorescent tdTomato-positive SST+ neurons in the ACC from WT (left, black) and SST-*Nrxn3* KO (right, red) mice. (**D**) IO curve of averaged frequency of AP firing at different step current injections from SST+ cells from WT (*n* =20, black) and SST-*Nrxn3* KO (*n* =20, red) mice.

Supplemental Figure 5

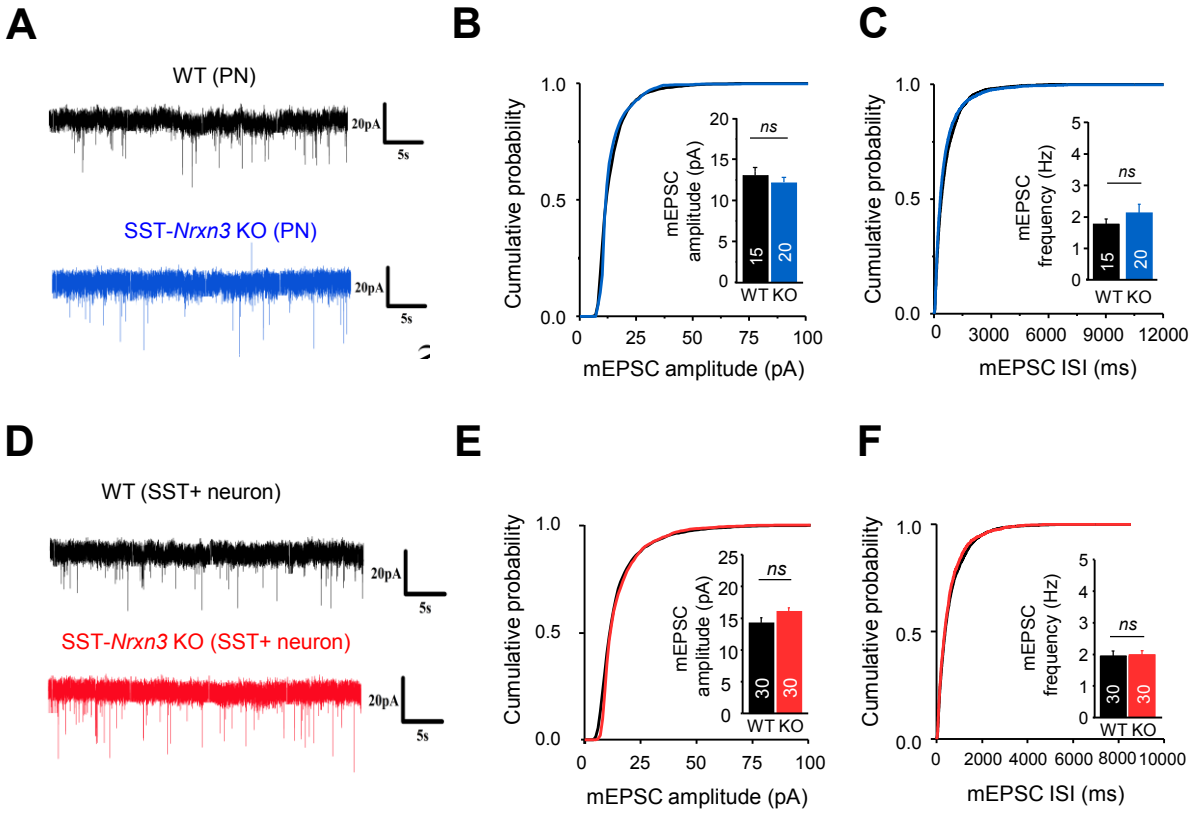

Supplemental Figure 5, Related to Figure 5. **Miniature excitatory synaptic transmission in SST-*Nrxn3* KO mice.** (**A**) Representative traces of miniature excitatory postsynaptic currents (mEPSCs) in pyramidal neurons (PN) from WT controls (top, black) and SST-*Nrxn3* KO (bottom, blue) mice. (**B**) Cumulative probability plot of mEPSCs amplitudes in PNs, and a summary graph of the mean mEPSC amplitude (inset) recorded from WT (n =15 cells) and SST-*Nrxn3* KO (n = 20) mice. (**C**) Cumulative probability plot of mEPSCs inter-spike-intervals (ISI) in PNs, and a summary graph of the mean mEPSC frequency (inset) recorded from WT (n =15 cells) and SST-*Nrxn3* KO (n =20) mice. (**D**) Representative traces of mEPSCs in tdTomato-positive SST+ neurons from WT control (top, black) and SST-*Nrxn3* KO (bottom, red) mice. (**E, F**) Cumulative probability plot of amplitudes and ISI of mEPSCs recorded in SST+ neurons from WT (n =30 cells) and SST-*Nrxn3* KO (n =30) mice. The insets show summary graphs of the mean amplitude and frequency of mEPSC.

Supplemental Figure 6

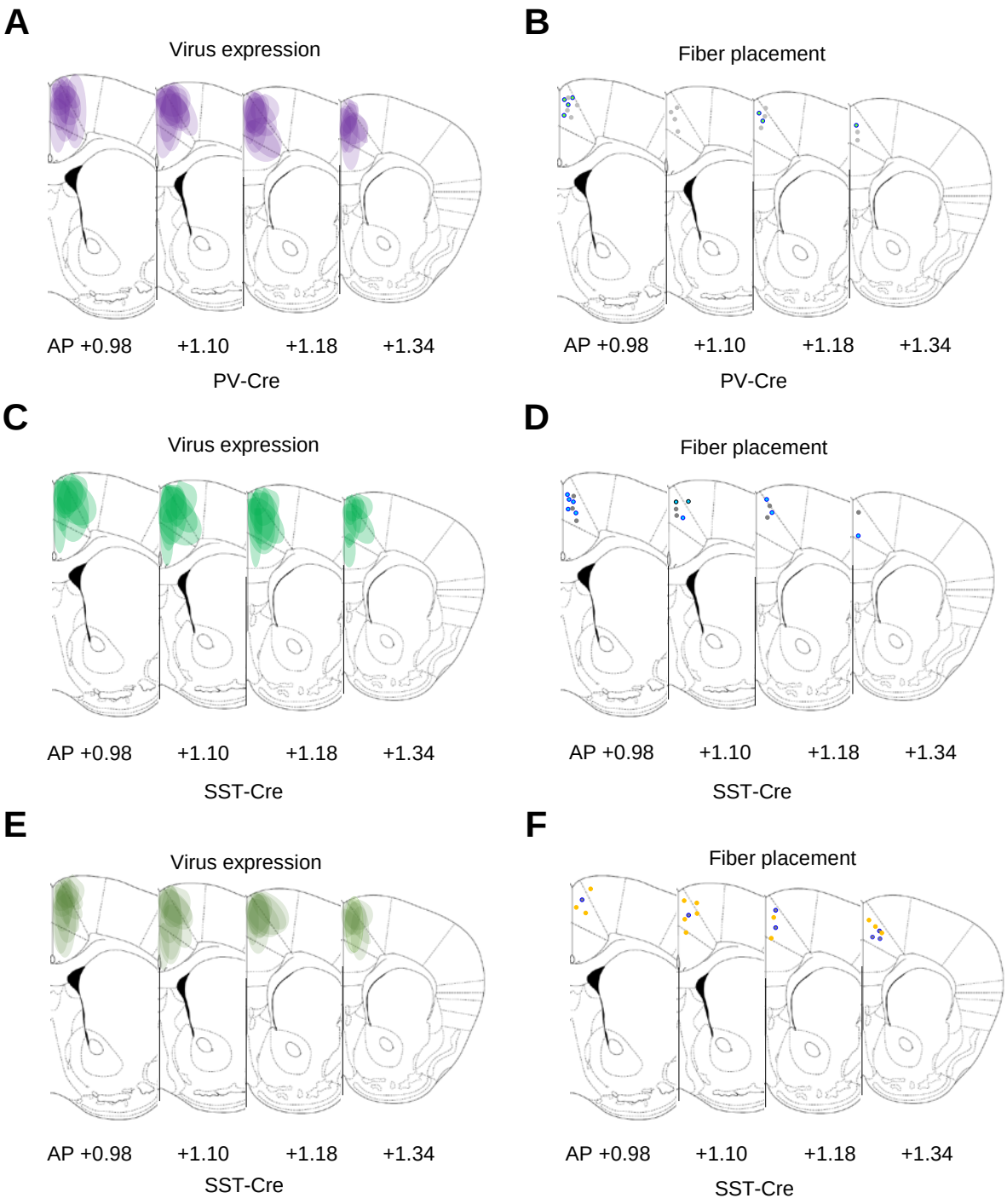

Supplemental Figure 6, Related to Figure 6. (**A**) Expression of AAV-DIO-NpHR-YFP throughout the right ACC in consecutive coronal brain sections in PV-Cre mice. (**B**) Fiber placements in PV-Cre mice of all experimental NpHR (blue circle) and control groups (gray circle). (**C**) Expression of AAV-DIO-NpHR-YFP throughout the right ACC in consecutive coronal brain sections in SST-Cre mice. (**D**) Fiber placements in SST-Cre mice of all experimental NpHR (blue circle) and control groups (gray circle). (**E**) Expression of AAV-DIO-ChR-YFP throughout the right ACC in consecutive coronal brain sections in SST-Cre mice. (**F**) Fiber placements in SST-Cre mice of all experimental ChR (yellow) and control groups (blue).

Supplemental Figure 7

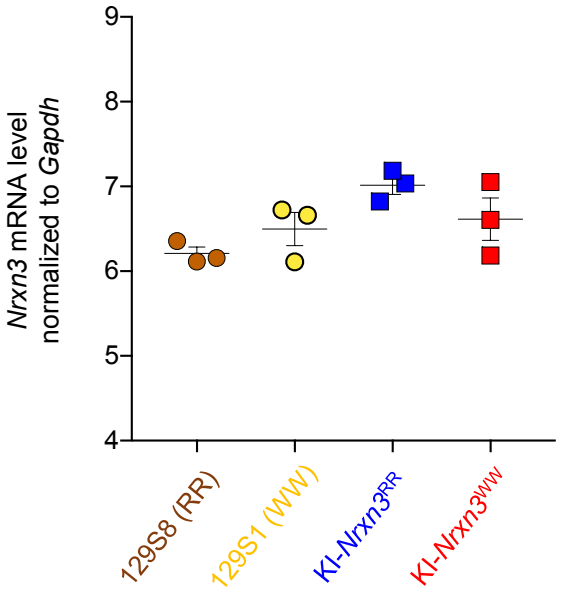

Supplemental Figure 7, Related to Figure 3 and Discussion. mRNA levels of *Nrxn3* in adult frontal cortex from 129S1, 129S8, KI-*Nrxn3*^{RR} (WT), and KI-*Nrxn3*^{WW} mice as determined by TaqMan gene expression assay. *Nrxn3* mRNA levels are normalized to *Gapdh* control and each dot represents a mean value of triplicated samples from a single animal. Error bars: ± s.e.m.